SCIENCE CHINA
Chemistry

•REVIEWS•

April 2023 Vol.66 No.4: 943–965
https://doi.org/10.1007/s11426-022-1448-8

Rational design and synthesis of advanced metal-organic frameworks for electrocatalytic water splitting

Yu-Jia Tang[1] & Ya-Qian Lan[2*]

[1]*School of Chemistry and Materials Science, Institute of Advanced Materials and Flexible Electronics (IAMFE), Nanjing University of Information Science and Technology, Nanjing 210044, China;*
[2]*School of Chemistry, South China Normal University, Guangzhou 510006, China*

Received September 21, 2022; accepted November 02, 2022; published online February 28, 2023

As a promising and significant technology for hydrogen production, electrocatalytic water splitting is a research hotspot in the energy conversion field for alleviating the global energy crisis and achieving carbon neutrality goals. Metal-organic frameworks (MOFs) have been widely investigated as catalyst candidates with remarkable activity and long-term electrocatalysis durability owing to their precise and tailorable structures: tunable pore channels in the range of micropore/mesopore promote the mass/electron transfer; high specific surface areas expose abundant active species; modified metal nodes can serve as active sites; versatile organic ligands can be functionalized to further enhance the electrocatalytic activity. In this review, recent advances in the rational design and synthesis of advanced MOF electrocatalysts for water splitting are presented in the following aspects. First, we analyze the design concepts of MOF electrocatalysts from the perspective of their distinct and modifiable structures. Second, three common synthesis techniques of MOF electrocatalysts are briefly introduced. Third, we focus on the classification of different MOFs for robust electrocatalytic water splitting, including pristine MOFs, mixed-metallic MOFs, MOF nanosheets, electrically conductive MOFs, MOFs on substrates, and polyoxometalate-based MOFs. Finally, summary and outlook are proposed to uncover the next generation of advanced MOFs for electrochemical energy conversion applications.

metal-organic frameworks, water splitting, electrocatalysis, hydrogen evolution reaction, oxygen evolution reaction, polyoxometalates

Citation: Tang YJ, Lan YQ. Rational design and synthesis of advanced metal-organic frameworks for electrocatalytic water splitting. *Sci China Chem*, 2023, 66: 943–965, https://doi.org/10.1007/s11426-022-1448-8

1 Introduction

With the growing global energy crisis and enormous carbon emissions, developing clean, sustainable, and renewable energy is concerned urgently [1,2]. Electrocatalytic water splitting has been considered as a potential technology for the conversion of electrical energy to hydrogen gas (H_2), which is a clean energy carrier to replace traditional fossil fuels for the benefit of our society in the near future [3–6]. Containing two half-reactions of hydrogen evolution reaction (HER) and oxygen evolution reaction (OER), electrocatalytic water splitting needs a standard potential of 1.23 V *vs*. reversible hydrogen electrode (RHE) due to its thermodynamics Gibbs free energy of ~237.2 kJ mol^{-1} [7]. However, the reaction usually needs to be driven at an actual voltage much higher than 1.23 V due to the existence of large kinetic barriers [8]. Therefore, to reduce overpotentials (η) in HER and OER, a high-efficient electrocatalyst can be loaded on the surface of a conductive support to form adsorption intermediates, promoting charge transfer between them during the electrocatalysis process. Currently, commercial Pt/C is a benchmark catalyst for HER while IrO_2 and RuO_2 are utilized as efficient OER electrocatalysts [9,10]. Unfortunately, scarcity, high cost, and instability of the noble-

*Corresponding author (email: yqlan@m.scnu.edu.cn)

metal-based electrocatalysts limit their wide industrial applications. At present, some research progress on non-noble-metal-based HER or OER electrocatalysts has been made, whereas problems of sluggish kinetics, large overpotentials, and short stability are widespread in these reported catalysts. Hence, developing electrocatalysts with low cost, high efficiency, and good durability for enhanced water splitting is still a significant challenge [11–16].

Metal-organic frameworks (MOFs), assembled by metal ions/clusters and organic ligands through coordination bonds, are a new class of porous crystalline materials with well-defined structures and multi-dimensional periodic lattices [17–20]. Since originally synthesized in the 1990s, MOFs have captured much attention by scientific researchers, exhibiting potential applications in various fields, such as catalysis [21–23], gas adsorption and separation [24], sensing [25], drug delivery [26], and proton conductivity [27]. Specifically, MOFs have been investigated in a key application area of electrocatalytic water splitting owing to their following distinct structural and compositional advantages. (i) Conspicuous porosity: owing to the adjustable length of organic ligands and various metal nodes, MOFs possess highly ordered micropores/mesopores and large surface areas, which can provide a high concentration of accessible active sites for accelerated electron transfer [28]. (ii) Various morphologies: MOFs with different morphologies can be prepared with specific raw materials by controlling their synthesis conditions. To date, various structures of MOFs have been reported to optimize their electrocatalytic activities, such as nanoparticles, nanowires, nanosheets, arrays, core-shell structures, and hollow structures [29]. (iii) Tunable metal nodes: transition metals of Fe, Co, Ni, Cu, Zn, Mn, Mo, *etc*., are commonly selected to construct active metal nodes [30,31]. In most cases, multi-metallic MOFs, such as binary and ternary metallic MOFs, can be designed to further improve their electrocatalytic properties. (iv) Easily functionalized ligands: organic ligands can also be modified with some active functional groups (*e.g*., −OH, −COOH, $-NH_2$) to change their compositions or coordinate with metal ion species to form new active sites. Despite the above-mentioned advantages, most MOF crystals still suffer from low conductivity, poor structural stability, and unsatisfactory activity in the electrocatalysis fields. Therefore, the guidance of design concepts to avoid the above shortcomings and further optimize structures and compositions is needed to prepare high-efficient MOF electrocatalysts for water splitting, which is presented in detail in Section 2.

Although many reviews about MOFs in electrocatalysis applications have been reported in the past few years [32–34], most of them mainly focus on discussions about water splitting mechanisms, MOF classifications at different dimensions, MOF-derived materials, and different electrocatalytic reactions. Few reviews have analyzed MOF electrocatalysts from the perspective of design concepts of structures, compositions, morphologies, synthesis strategies, *etc*., which can provide practical guidance to prepare high-efficient MOFs for HER and OER. Considering the importance of the structure-property relationship of an electrocatalyst, an instructive review summarizing design concepts, synthesis techniques, and classifications of MOF electrocatalysts for water splitting is necessary to provide us insights and guidance for further investigations. In this review, recent progress of the rational design and synthesis of advanced MOFs for efficient electrocatalytic water splitting is provided (Scheme 1). Firstly, design concepts of MOF electrocatalysts from the points of precise structure modulation, regulation of MOF dimensions, metal nodes/ligands modifications, and structural reconstruction are presented. Secondly, we demonstrate three representative synthesis methods of MOF electrocatalysts for water splitting. Then, six types of MOF electrocatalysts are divided to discuss their structures and electrocatalytic performances for HER and OER in detail. Finally, we summarize and analyze perspectives and challenges, providing specific guidelines to design robust MOF electrocatalysts for water splitting. We hope this review will offer scientific researchers available inspiration for studying in electrocatalysis applications.

2 Design concepts of MOF electrocatalysts

Owing to tunable porous structures, diverse topologies, large specific surface areas, active metal nodes, and functionalized organic linkers, MOFs show booming development in the field of electrocatalytic water splitting. However, most of the pristine MOF crystals possess unstable structures, low conductivities, and limited active sites, resulting in insufficient electrocatalytic performance in harsh media. In this section, we focus on the rational design concepts of MOFs as high-efficient electrocatalysts for water splitting from the perspective of their unique structural features.

2.1 Precise structure modulation

Compared with the traditional porous materials of active carbon and molecular sieve, MOFs can be rationally designed with special structures and well-defined porosity. On one hand, the precise structures of the as-synthesized MOF crystals can be determined by single-crystal X-ray diffraction (XRD) analysis, providing direct evidence for the structure-property relationships. For instance, Liao and Zhang *et al*. [35] synthesized a hybrid **Fe_3-Co_2** MOF of which the open metal sites-contained $\{Fe_3(\mu_3\text{-}O)(bdc)_3\}_4$ framework could bind to the $Co_2(na)_4(L^T)_2$ cluster. Due to its good chemical stability and unique Co coordination mode, **Fe_3-Co_2** exhibited enhanced electrocatalytic activity for

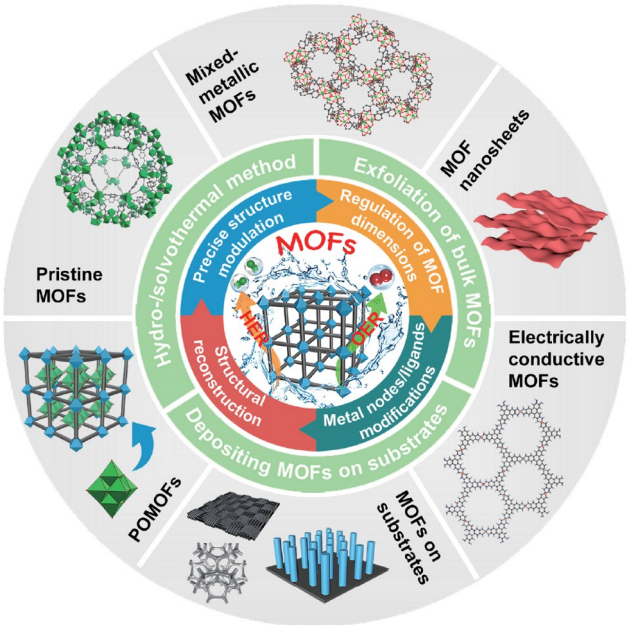

Scheme 1 Illustration of designing advanced MOF electrocatalysts for water splitting (color online).

OER. On the other hand, the intrinsic and high porosity of MOFs ensures large specific surface areas to facilitate the electron transfer. Moreover, different active species (single atoms, quantum dots, polyoxometalates, nanoclusters, metal complexes, *etc*.) can be embedded within pores/cavities or bonded to MOFs, thereby changing their porosity, structures, and chemical stabilities [36–38]. These encapsulated species or newly formed structures are regarded as active sites or auxiliary materials to improve the electrocatalytic performance for water splitting. Peng's research group [39] reported a series of nanohybrids with noble metal nanoparticles anchored on Ni-MOF (M@Ni-MOF, M = Ru, Pd, Ir) using a spontaneous redox method (Figure 1a). The quantum-sized metal nanoparticles were combined with the Ni-MOF *via* metal–oxygen bonds, producing active interfacial structures to improve its HER activity dramatically.

It can be seen that the periodic arrangement of metal nodes and organic units in MOFs makes certain of maximum exposure of well-dispersed active sites on metal sites. Combined with physical characterizations and theoretical analysis, it is beneficial to analyze the reaction mechanism and verify the active sites of these crystalline structured MOFs. Therefore, MOFs with precise structures are desirable candidates, which can be regulated accurately for the construction of highly efficient electrocatalysts for water splitting.

2.2 Regulation of MOF dimensions

MOFs have a high flexible regulation ability of coordination structures, leading to their structural variety in different dimensions. Recently, many studies have found that designing MOFs with specific morphologies at nano-/micro-scales, including zero-dimension (0D), one-dimension (1D), two-dimension (2D), and three-dimension (3D), can increase their conductivities and stabilities [29,40]. In general, 0D MOFs are particles with micro-/nano-sizes. Especially, MOF nanoparticles in a range of tens to hundreds nanometers are suggested to be synthesized because they have larger surface areas and more exposed active sites compared with the micro-sized MOF particles. 1D MOFs demonstrate various morphologies of nanorods, nanowires, nanotubes, nanofibers, *etc*., possessing short charge transfer pathways and large surface areas. The electrospinning and template methods have been used to prepare 1D MOFs, which cannot obtain pure MOFs due to the introduction of additives. Besides, it is still a challenge to control the synthesis of 1D MOFs with uniform and dispersed morphologies using a facile method. 3D MOFs possess abundant morphologies and hierarchical structures, which are beneficial to being optimized to improve the electrocatalytic activities. Notably, 3D MOFs with porous structures can expose active sites and accelerate charge transfer for electrocatalysis. Therefore, designing well-defined 3D MOFs with superior performance for water splitting deserves deep exploration.

Significantly, lowering structural dimensions to construct 2D MOFs is a brilliant choice to enhance their electrocatalytic activities [41,42]. The 2D MOFs have been widely reported as excellent electrocatalysts owing to the following advantages: (i) they have ultrathin nanosheet structures, which are in favour of the exposure of abundant active sites; (ii) the 2D MOF nanosheets can effectively speed up the charge/mass transfer during the electrocatalysis process; (iii) the atomic structures in the 2D MOFs can be modified facilely for further investigation of their relationship between structure and activity.

For example, Zhao and co-workers [43] described a universal strategy to prepare 2D NiFe-MOF nanosheet arrays on conductive supports, which possessed good activities for electrocatalytic water splitting due to the exposed metal sites, improved conductivity, and good hierarchical porosity. Li's research group [44] reported an Ni(II)-MOF nanosheet array ($Ni_2(OH)_2(BDC)$) with defected structures through an alkali-etched treatment. The alkaline corrosion in the KOH medium led partial break of Ni–O bonds along with the import of K^+ into the framework of Ni-MOF, forming rough and expanded layer structures (Figure 1b). The as-prepared defect-rich Ni-MOF nanosheet arrays (D-Ni-MOF NSA) had abundant unsaturated Ni active sites and enhanced conductivity, achieving good electrocatalytic performance with an overpotential (η_{10}) value of 219 mV at a current density of 10 mA cm^{-2} for OER and a η_{10} value of 101 mV for HER. Therefore, MOFs can be flexibly controlled with desired dimensional structures, such as nanoparticles, nanowires,

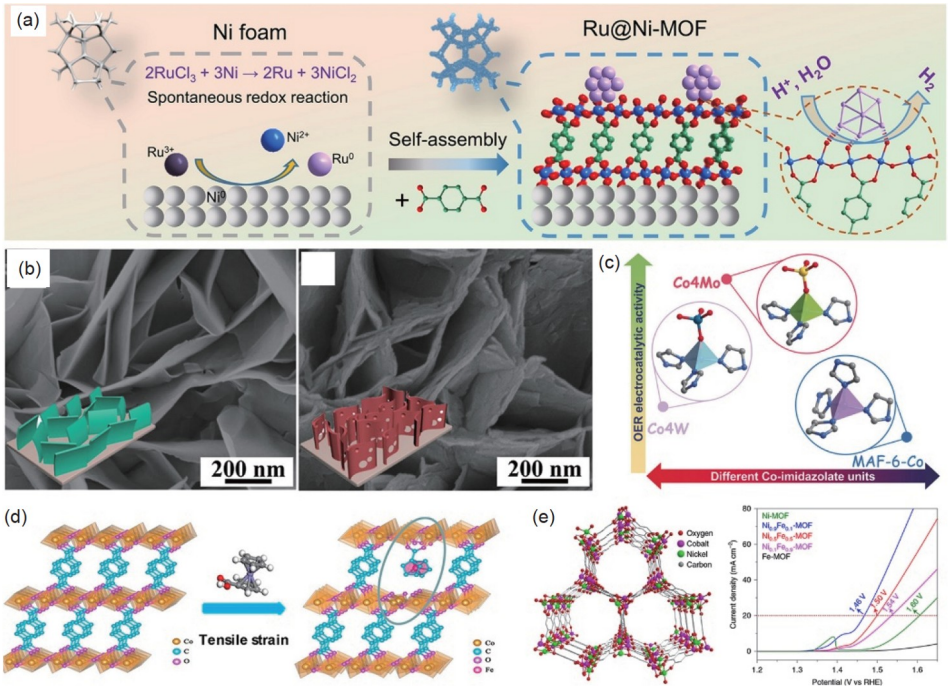

Figure 1 (a) Schematic illustration of M@Ni-MOF nanosheets on NF as HER electrocatalysts. Reproduced with permission from Ref. [39], copyright 2021 John Wiley & Sons, Inc. (b) SEM images of Ni-MOF and defect-rich Ni-MOF after alkali-etched treatment. Reproduced with permission from Ref. [44], copyright 2020 John Wiley & Sons, Inc. (c) Structures and OER comparison of **Co_4Mo**, **Co_4W**, and MAF-6-Co. Reproduced with permission from Ref. [47], copyright 2019 John Wiley & Sons, Inc. (d) Structures of CoBDC and CoBDC FcCA. Reproduced with permission from Ref. [51], copyright 2022 American Chemical Society. (e) Structure of $Ni_{0.5}Co_{0.5}$-MOF-74 and LSV curves of $Ni_{0.9}Fe_{0.1}$-MOF-74 and control samples for OER. Reproduced with permission from Ref. [55], copyright 2020 Springer Nature (color online).

nanosheets, nanospheres, nanocubes, and polyhedrons. These nano-sized MOFs with specific structures are one of the hot spots as outstanding candidates for electrocatalytic water splitting.

2.3 Modifications of metal nodes/ligands

It is well-known that structural modification is an effective strategy to modify metal nodes and organic ligands of MOFs at atomic levels. Two common methods of structural tuning of MOFs are as follows: (i) the metal nodes can be functionalized to form open multi-metal sites by introducing other active metals; (ii) the organic ligands can be modified to bond to other active species or form defects [21,29]. Consequently, the modifications of metal nodes/organic ligands of MOFs can modulate their compositions, pore sizes, electronic structures, and conductivities, providing abundant active sites for the enhancement of the intrinsic electrocatalytic activity for water splitting.

On one hand, doping specific or more kinds of metals with optimized molar ratios can obtain mixed-metal node centers with multiple valences. The multi-metal nodes are regarded as active sites to improve MOFs' electrocatalytic activity [45,46]. In 2019, Zhang's research group [47] synthesized two non-3d metal-modulated cobalt imidazolate frameworks of $Co_4(MO)_4(eim)_6$ (M = Mo or W, Heim = 2-ethylimidazole) with $Co(eim)_3(MO_4)$ units and good water stability (Figure 1c). The introduction of the non-3d metals of Mo and W tailored the electronic structures of Co centers and increased the reactant/product affinity for electrocatalysis. The Mo-modulated MOF of Co_4Mo showed excellent OER performance with an overpotential of 210 mV at 1 mA cm^{-2} in the CO_2-saturated 0.5 M $KHCO_3$ solution and an overpotential of 388 mV at 2 mA cm^{-2} in a phosphate buffer solution.

On the other hand, organic ligand modifications are able to regulate the electronic structures of MOFs. Introducing functional groups (*e.g.*, −OH, $-SO_3$) in the terminal of ligands can effectively change the structural environments of metal ions [48,49]. In addition, partially substituted or missing linkers also can affect coordination environments, change electronic structures, and form defective ligand sites in MOFs [50,51]. For example, Wang's research group [52] employed a dielectric barrier discharge plasma etching method to create coordinately unsaturated metal sites (CUMSs) with missing ligands in ZIF-67. The plasma-treated ZIF-67 had enhanced OER activity because the rich CUMSs served as active sites. In 2022, He *et al.* [51] reported an ultrathin CoBDC FcCA nanosheet catalyst, which had a bifunctional microreactor containing Co active sites and ferrocene carboxylic acid (FcCA) ligands *via* the partial substitution of cobalt-terephthalic acid (CoBDC) to the

FcCA ligands (Figure 1d). The coordination of Co active moieties and FcCA ligands forming the microreactor of tensile strain could optimize the Co spin state and enhance the formation of O–O bond. The CoBDC FcCA nanosheets demonstrated a low η_{10} value of 280 mV and a small Tafel slope of 53 mV dec^{-1} for OER. Very recently, Gao *et al*. [53] constructed an MCl_2@Th-MOF crystal (M = Cu, Co, Ni) containing an MN_2Cl_2 coordination geometry, which was strongly chelate-coordinated by MCl_2 and bipyridine N in the 2,2′-bipyridine-5,5′-dicarboxylic acid (BPYDC) ligand. Combined with the single-crystal XRD and theoretical calculations, the as-prepared single-metal-site in MCl_2@Th-MOF showed an unusual semirigid structure due to the two rotatable charge-balance Cl^- anions. Remarkably, $CoCl_2$@Th-MOF demonstrated an enhanced OER performance in an acidic medium with a η_{10} value of 388 mV and a Tafel slope of 94 mV dec^{-1}, attributing to the robust Th-MOF support and strong coordination bond of Co–N in the semirigid single-site. Still, these studies about ligand modifications in MOF electrocatalysts are less reported and need further investigation. Therefore, the modifications of open metal nodes and organic ligands not only increase the diversity of MOF structures but also are feasible routes to effectively boost their electrocatalytic performance for water splitting.

2.4 Structural reconstruction

The chemical stability of MOFs in acidic, neutral, and alkaline electrolytes is an important factor for electrocatalysis applications [54]. The evaluation criteria for MOF stability are their structural integrity ability in which some kinetic factors are considered, including linker rigidity, surface hydrophobicity, pore size, coordination number, and metal valence. However, in some cases for OER, MOFs are unstable and structurally transformed partially or totally to new species, leading to changes in the coordination environments. These unstable MOFs are recognized as "pre-catalysts", which are *in situ* structurally reconstructed to form real active intermediates (*e.g*., metal oxyhydroxides and oxides) when being electrolyzed in a harsh electrolyte [55,56]. Interestingly, intrinsic properties of precise structures, high porosities, and diverse compositions of these MOF pre-catalysts have an impact on their reconstruction process, thereby acquiring many active species on the surface and further enhancing their activity and durability [57,58].

Recently, scientific researchers focused on the structural transformation of MOF electrocatalysts through multiple *in situ* characterizations and theoretical calculations [59,60]. For instance, Tang and co-workers [55] utilized $Ni_{0.5}Co_{0.5}$-MOF-74 as an OER electrocatalyst, which was structurally transformed to $Ni_{0.5}Co_{0.5}OOH_{0.75}$ at the Ni and Co nodes according to the operando X-ray absorption spectroscopy (XAS) analysis (Figure 1e). The as-formed $Ni_{0.5}Co_{0.5}$-$OOH_{0.75}$ species involved abundant oxygen vacancies with unsaturated coordination and increased valence states of Co/Ni. In particular, $Ni_{0.9}Fe_{0.1}$-MOF-74 with an optimized Ni/Fe molar ratio delivered a low η_{10} value of 198 mV and a high turnover frequency (TOF) of ~0.95 s^{-1} at an overpotential of 0.3 V for OER. In 2022, Zhang *et al*. [61] synthesized a trimetallic FeCoNiBTC MOF on Ni foam (NF) as the OER working electrode facilely. The FeCoNiBTC pre-catalyst was phase-transformed to $FeCoNiO_x(OH)_y$ during the alkaline water oxidation process according to *in situ* Raman characterization results. Theoretical analysis indicated that the as-formed $FeCoNiO_x(OH)_y$ species possessed real active metal sites with optimized electronic structures and appropriate energy barriers for the breaking of *OH and the formation of *OOH during OER.

It is worth mentioning that structural transformation between MOFs and layer double hydroxides (LDHs) is also a promising strategy to prepare high-efficient MOF electrocatalysts for water splitting. On one hand, the morphology of MOFs can be well controlled using LDHs as precursors. LDHs are ultrathin layered nanosheets for the uniform epitaxial growth of 2D MOFs, which contain abundant exposed active sites for accelerated charge transfer [62]. On the other hand, some MOFs are unstable and can serve as direct templates, which transform to LDHs during the electrochemical oxidation process [63]. These MOF-derived LDH nanosheets usually exhibit excellent performance due to the existence of abundant coordinatively unsaturated active sites and defects when compared with the traditional LDHs with inert planes and aggregated morphologies. In addition, partial structural transformation of LDHs to MOFs and *vice versa* can prepare MOF/LDH composites [64,65]. When serving as electrocatalysts for water splitting, the MOF/LDH composites combine advantages from both MOFs and LDHs, including porous structures, good conductivities, dispersed nanosheet morphologies, and exposed active metal sites.

As we know, MOFs generally experience structural evolution during OER. Some attention should also be paid to the structure evolution of MOFs during the HER electrocatalysis process to discover the real active species or structures. Unfortunately, scientific researchers do not consider it in most cases. Some MOFs show structural and compositional stabilities without changes during HER according to the after stability physical characterizations [66,67]. Moreover, some reports have investigated the structural evolution for HER in detail to verify the real active species. For example, Zhou *et al*. [45] reported trimetallic Mn_xFe_yNi-MOF-74 films on NF as efficient HER and OER electrocatalysts. The high-valent Mn and Fe species helped to stabilize the metal sites and modulate the electronic structures for enhanced electrocatalytic activities. According to the X-ray photoelectron

spectroscopy (XPS) analysis after HER, they found that Mn^{4+} was partially reduced to Mn^{3+}, increasing the contents of Fe^{3+} and Mn^{3+} species. Therefore, after the HER stability test, the electronic structures of Mn_xFe_yNi-MOF-74 films were changed. Chen *et al*. [68] proposed chiral macromolecular trimetallic MOFs with 6% lattice expansion on NF (LS-CMMOFs/NF) as efficient HER and OER electrocatalysts. The morphology and structure of 6%LS-CMMOFs/NF demonstrated no obvious changes after the long-term HER stability test, according to the XRD, scanning electron microscope (SEM), and high-resolution transmission electron microscope (HRTEM) results. However, XPS and *in situ* Raman characterizations suggested that the newly formed metal nitrides of Ni/Co-N were the active centers for HER. Therefore, some studies have found that valence states of metals in MOFs were changed for facilitated charge transfer, and new species were formed during HER. We think that scientific researchers should draw attention to the structural evolution of MOFs during HER.

In brief, the structural transformation of MOFs should be taken into consideration because the structural collapse often happens to produce new active components. Meanwhile, combined with proper *in situ* and *ex situ* characterization technologies, we can identify the real active sites and analyze the transformation process for water splitting.

3 Synthesis techniques of MOFs for water splitting

Typically, different synthesis techniques have different advantages and disadvantages, which can affect MOFs' crystalline structures, porosities, particle sizes, yields, and further properties [69]. In the past decades, versatile synthesis methods have been developed to design and construct MOFs with active chemical components, controlled morphologies, and good conductivities for electrochemical applications, for example, hydro-/solvothermal method, exfoliation method, template method, ultrasonic method, microwave-assisted method, mechanochemical method, electrochemical method, and depositing MOFs on substrates [70,71]. In this section, we briefly introduce three commonly used synthesis methods of MOFs in electrocatalytic water splitting applications.

3.1 Hydro-/solvothermal method

The hydro-/solvothermal method is a conventional strategy for the preparation of MOF crystals. It is carried out in a closed system with the utilization of high temperature, high pressure, specific molar ratio of starting materials, long reaction time, and solvents. MOFs prepared using this method usually have high porosities, good thermal and chemical stabilities but large crystal sizes and poor conductivities, which are not quite suitable for electrocatalysis. To reduce the particle sizes of MOFs, modulators (*e.g.*, acetic acid and benzoic acid) can be introduced into the reaction system to regulate their morphologies. These small-sized MOFs, especially nano-MOFs, are potential candidates as high-performed electrocatalysts for HER and OER.

For instance, Chen *et al*. [72] reported a series of isostructural MOFs by a solvothermal reaction. These MOFs were assembled using V-shaped metal-oxygen clusters as metal nodes, which contained both open metal sites and coordination-saturated metal sites. The precise modulation of Fe/Ni in the clusters could be determined by XRD, Mössbauer spectroscopy, and inductively coupled plasma-mass spectrometry analyses. The as-synthesized $Ni_{3(1-x)}Fe_{3x}$-MOF showed good electrocatalytic performance for HER and OER owing to the precise structures with unsaturated metal sites.

3.2 Exfoliation of bulk MOFs

2D MOFs have a fundamental role in electrochemical applications due to their ultrathin morphologies, enhanced conductivities, and abundant exposed active sites [73–75]. Typically, two main methods have been developed to prepare 2D MOF nanosheets: (i) bottom-up method, using a certain crystal synthesis method to directly assemble 2D MOFs from metal ions and organic ligands; (ii) top-down method, using an appropriate exfoliation strategy to obtain 2D nanosheets from bulk MOFs, including physical, chemical, and electrochemical exfoliations. For the bottom-up method, the surfactants (*e.g.*, polyvinylpyrrolidone (PVP), hexadecylcetyltrimethylammonium bromide (CTAB), and sodium dodecyl sulfate (SDS)) are usually used to control the nucleation and growth of 2D MOFs. However, the incomplete removal of these surfactants may lead to the blocking of active sites. Hence, the growth direction of 2D MOFs should be strictly controlled by this method. For example, Lang and co-workers [75] prepared a series of bimetallic Ni-based MOF nanosheets (Ni-M-MOF NSs, M = Al, Mn, Zn, Co, and Cd) using a bottom-up solvothermal method. The mixed solvents of *N*,*N*-dimethylacetamide and water could effectively control the growth of 2D MOF NSs with two or three layers. The ultrathin nanosheet morphology of Ni-Fe-MOF ensured well-exposure of active sites and acceleration of charge transfer, leading to its good electrocatalytic performance for OER. Furthermore, 2D MOFs prepared by the top-down methods, such as ball milling and ultrasonication, often suffer from fragmentary nanosheets and low exfoliation efficiency, resulting in a decrease in the electrocatalytic efficiency to some extent. This is because the relatively strong interactions within MOFs are van der Waals forces or hydrogen bonds in most cases. Since 2D MOFs have widely served as high-efficient electrocatalysts, we

should choose an appropriate and optimized synthesis route for the design of 2D MOFs with uniform thin nanosheet structures.

3.3 Depositing MOFs on substrates

Depositing MOFs on conductive substrates is one of the most efficient and novel strategies for the preparation of MOF electrocatalysts. In general, metal foams, metal foils, and carbon-based supports are selected as ideal and conductive substrates for the *in situ* homogeneous growth of MOFs [76–78]. The two common growth conditions are hydrothermal and electrodeposition reactions under a relatively mild condition, obtaining nano-/micro-sized MOFs with various array structures on substrates, such as nanoparticles, nanorods, nanosheets, and other specific 3D architectures. Liu and Tse *et al*. [79] synthesized 2D NiFc-MOF nanosheet arrays *in situ* on a nickel foam (NF) substrate using a typical solvothermal method. The NiPc-MOF nanosheets were assembled by nickel salts and 1,1′-ferrocenedicarboxylic acid, which were grown on the NF skeleton vertically and uniformly. Due to the vertically oriented 2D morphology, the NiFc-MOF/NF showed enhanced OER performance in an alkaline medium. Moreover, some MOFs (*e.g.*, ZIF-67, HKUST-1, and MOF-74) grown on the substrates can take place on a short time scale at room temperature, which is regarded as an eco-friendly and high-efficient process. Therefore, depositing MOFs on substrates allows precise control of size, morphology, and loading mass, enabling rapid mass/electron transfer of the as-prepared MOF/substrates as direct working electrodes for electrocatalysis.

4 Classification of MOFs for water splitting

MOFs have been widely investigated as high-efficient water splitting electrocatalysts due to the multiple advantages mentioned above. In this part, we highlight recent advances of MOF electrocatalysts for HER and OER, which are classified into the following six types: pristine MOFs, mixed-metallic MOFs, MOF nanosheets, electrically conductive MOFs, MOFs on substrates, and polyoxometalate-based MOFs. The structure-activity relationships for the representative MOF electrocatalysts are discussed here emphatically. Their electrochemical water splitting performances of HER and OER are presented in Tables 1 and 2, respectively, which contain critical electrocatalytic parameters of electrolyte, substrate, overpotential, Tafel slope, and stability.

4.1 Pristine MOFs

In the early years, pristine MOFs have been widely used in photocatalytic systems [80,81], while their electrocatalytic water splitting application has been reported in popularity in recent years. In this category, pristine MOFs serving as water splitting electrocatalysts are crystalline particles or powders with determined structures but no further modifications of structures or components. These pristine MOFs need to be mixed with conductive agents and then loaded on glassy-carbon electrodes or other conductive supports for measurement due to their intrinsic poor conductivities and large particle sizes. For example, Li and co-workers [82] reported two polymorphic Co(II) MOFs (CTGU-5 and -6) using different surfactants (Figure 2a). CTGU-5 showed a layered structure with water molecules coordinated with the Co site, while CTGU-6 featured a 3D framework in which H_2O was hydrogen-bonded to the MOF as the lattice molecule. Remarkably, CTGU-5 mixed with acetylene black of AB&CTGU-5 (4:1) exhibited good HER performance with an ultralow onset overpotential of 18 mV, a low η_{10} value of 44 mV, a Tafel slope of 45 mV dec^{-1}, a high exchange current density (j_0) value of 8.6 × 10^{-4} mA cm^{-2}, and long-term durability over 96 h in an acidic medium (Figure 2b). Computational studies revealed that the unpaired electron and empty E_g orbit of Co could trap proton and electron, thus promoting the HER activity significantly (Figure 2c). Bucci *et al*. [83] described two imidazolate-based Co-MOFs possessing different peripheral groups of −Me for IFP-5 and −OMe for IFP-8. IFP-8 presented good electrocatalytic performance toward OER with a lower η_{10} value of 319 mV than that of IFP-5 and a nearly 100% Faradaic yield of O_2 due to the influence of the −R groups. Combing with XRD, attenuated total reflection (ATR), and extended X-ray absorption fine structure (EXAFS) characterizations, the frameworks were completely degraded to form CoOOH species after the long-term stability experiment.

It is can be seen that a pristine MOF crystal often bears restricted electrocatalytic activity for water splitting due to intrinsically poor active sites and low conductivities. Fortunately, combing different MOFs to form a hybrid MOF material is a feasible route to optimize the electrocatalytic behavior. For instance, Bu's research group [84] proposed a straightforward sonication method to synthesize a uniform mixture of lamellar Ni-MOFs attached to the surface of the octahedral Fe-MOFs (Fe-MOFs@Ni-MOFs) (Figure 2d, e). The optimized Fe-MOFs@Ni-MOFs had a low η_{10} value of 275 mV and a Tafel slope of 56.7 mV dec^{-1} for OER due to the synergistic effect between the two MOFs (Figure 2f). According to *ex situ* TEM and XRD characterizations, they found that the organic ligands in Fe-MOFs@Ni-MOFs were substituted by hydroxyl ions to form active NiFe-LDH sheets and rich defects on its surface during the electrocatalysis process (Figure 2g). In 2022, Kaner and co-workers [85] introduced a layer-by-layer assemble strategy to prepare a trimetallic Fe–Co–Ni MOF on NF under a reductive elec-

Table 1 Summary of representative MOF electrocatalysts for HER

Sample ID	Electrolyte	Substrate	Overpotential	Tafel slope (mV dec^{-1})	Stability
Ni-BTC [31]	0.5 M H_2SO_4	Carbon fiber paper	53 mV@−10 mA cm^{-2}	62	12 h@−0.25 V *vs.* RHE
$[Co_2(3,3'\text{-bpy})(3,5\text{-bpp})(4,3'\text{-bpy})](H_2O)_3[SiW_{12}O_{40}]$ [36]	1 M KOH	NF [a]	92 mV@−10 mA cm^{-2}	92.1	48 h@−10 mA cm^{-2}
D-Ni-MOF NSA [44]	1 M KOH	Ni foil	101 mV@−10 mA cm^{-2}	50.9	N/A [f]
$Mn_{0.52}Fe_{0.71}$Ni-MOF-74 [45]	1 M KOH	NF	99 mV@−10 mA cm^{-2}	103.8	100 h@−10 mA cm^{-2}
Fe_2Zn-MOF [46]	0.1 M KOH	NF	221 mV@−10 mA cm^{-2}	174	N/A
NH_2-MIL-88B(Fe_2Ni) MOF [66]	1 M KOH	NF	87 mV@−10 mA cm^{-2}	35.2	30 h@ −500 mA cm^{-2}
$Ni_3(Ni_3$•HAHATN$)_2$ [67]	0.1 M KOH	RDE [b]	115 mV@−10 mA cm^{-2}	45	Maintaining at −10 mA cm^{-2} for 10 h
6%LS-CMMOFs [68]	1 M KOH	NF	100 mV@−10 mA cm^{-2}	72	100 h@−10 mA cm^{-2}
Ni_1Fe_2-MOF [72]	0.1 M KOH	NF	155 mV@−10 mA cm^{-2}	71	N/A
MFN-MOFs(2:1) [76]	1 M KOH	NF	79 mV@−10 mA cm^{-2}	30.1	N/A
HKUST-1 ED [77]	0.5 M H_2SO_4	CC [c]	590 mV@−10 mA cm^{-2}	183.6	12 h at a fixed voltage
AB&CTGU-5 (1:4) [82]	0.5 M H_2SO_4	GCE [d]	44 mV@−10 mA cm^{-2}	45	96 h@−0.255 V *vs.* RHE
Fe-Co-Ni MOF [85]	1 M KOH	NF	116 mV@−10 mA cm^{-2}	56	48 h@−0.1 V *vs.* RHE
Co/Cu-MOF [94]	1 M KOH	GCE	391 mV@−10 mA cm^{-2}	94	14 h@−0.38 V *vs.* RHE
NiYCe-MOF [106]	1 M KOH	NF	136 mV@−10 mA cm^{-2}	74	100 h@−50 mA cm^{-2}
NiFe-MOF array [117]	1 M KOH	NF	68 mV@−10 mA cm^{-2}	112	20 h@−0.17 V *vs.* RHE
Cu-BHT [123]	0.5 M H_2SO_4	GCE	450 mV@−10 mA cm^{-2}	95	20 h@−0.7 V *vs.* SHE
O_v-Fe MOF [138]	1 M KOH	Fe foam	72 mV@−10 mA cm^{-2}	65	50 h@−10 mA cm^{-2}
NENU-500 [146]	0.5 M H_2SO_4	GCE	237 mV@−10 mA cm^{-2}	96	N/A
ZnMo-POMOF [147]	0.5 M H_2SO_4	NF	180 mV@−10 mA cm^{-2}	66	3,000 s at a certain potential
HUST-200 [148]	Acidic medium	GCE	88 mV@−10 mA cm^{-2}	51	N/A
Co-MOF [150]	0.5 M H_2SO_4	GCE	357 mV@−10 mA cm^{-2}	107	96 h@−0.357 V *vs.* RHE
Cu[Ni(pdt)$_2$] [151]	pH 1.3 solution	RDE	530 mV@−10 mA cm^{-2}	69.0	120 min@−0.50 V *vs.* RHE
$[TBA]_3[H_4PMo_8^{V}Mo_4^{VI}O_{40}Zn_4](HTPT)_2$ [152]	0.5 M H_2SO_4	CP [e]	417 mV@−10 mA cm^{-2}	68	10 h@−0.417 V *vs.* RHE
NiFe-MOF-74 [153]	1 M KOH	NF	195 mV@−10 mA cm^{-2}	136	15 h at a certain potential
Mg_2V-MOF [154]	1 M KOH	NF	195 mV@−10 mA cm^{-2}	174	5,000 s at a certain potential

a) NF means Ni foam; b) RDE means rotating disk glassy carbon electrode; c) CC means carbon cloth; d) GCE means glassy carbon electrode; e) CP means carbon paper; f) N/A means not available.

trodeposition condition (Figure 2h). The Fe–Co–Ni MOF had a unique tri-layer morphology because metal nodes in each layer were linked by the 2-amino-1,4-benzenedicarboxylic acid (BDC-NH_2) ligand. Notably, Fe–Co–Ni MOF exhibited superior activities with η_{10} values of 116 mV for HER and 254 mV for OER in an alkaline medium (Figure 2i). Theoretical calculations revealed that the excellent electrocatalytic performance of Fe–Co–Ni MOF was attributed to the strong H_2O adsorption on its metal nodes that led to the efficient activation of the O–H bond.

Zhu and Xu *et al.* [86] reported a self-supporting MOF composite grown on an NiFe alloy foam support (NiFe-NFF) using a semisacrificial template method (Figure 3a). The NiFe foam served as both Ni/Fe metal sources and growth support. The NiFe-NFF composite showed a unique morphology that small-sized Fe-rich Fe(Ni)-MOF cluster particles were loaded on the surface of Ni-rich Ni(Fe)-MOF nanosheets uniformly (Figure 3b). The NiFe-NFF serving as a working electrode revealed an impressive OER performance with a η_{10} value of 227 mV due to the synergistic effect between Fe and Ni and its modulated electronic structures (Figure 3c). Similarly, Rui *et al.* [87] synthesized an Ni-MOF@Fe-MOF hybrid that Fe-MOF nanoparticles were electrochemically deposited on the Ni-MOF nanosheets (Figure 3d). Ni-MOF@Fe-MOF exhibited enhanced electrocatalytic performance for OER with a η_{10} value of 265 mV and a Tafel slope of 82 mV dec^{-1} in 1 M KOH (Figure 3e). During the OER process, the NiO nanograins and mesopores were formed as the active species while the structure of the original MOF hybrid was damaged completely according to the TEM and Raman characterization results (Figure 3f).

Therefore, the pristine MOF crystals have been directly utilized as electrocatalysts for HER and OER owing to their precise structures, large catalytic surface areas, and exposed active sites. The water splitting performances can be promoted by changing their crystalline structures or hybridization. However, poor electrical conductivity, structural instability, as well as limited active sites of MOFs must

Table 2 Summary of representative MOF electrocatalysts for OER

Sample ID	Electrolyte	Substrate	Overpotential	Tafel slope (mV dec^{-1})	Stability
Co_4Mo [47]	0.1 M PBS [a)]	GCE	388 mV@2 mA cm^{-2}	144	15 h@1.72 V *vs.* RHE
MAF-X27-OH [49]	1 M KOH	Cu foil	292 mV@10 mA cm^{-2}	88	24 h@10 mA cm^{-2}
CoBDC-Fc [50]	1 M KOH	NF	178 mV@10 mA cm^{-2}	51	80 h@100 mA cm^{-2}
$CoCl_2$@Th-BPYDC [53]	0.1 M $HClO_4$	CP	388 mV@10 mA cm^{-2}	94	25 h@1.681 V *vs.* RHE
$Ni_{0.9}Co_{0.1}$-MOF-74 [55]	1 M KOH	GCE	198 mV@10 mA cm^{-2}	N/A	N/A
Ni_1Fe_2-MOF [72]	0.1 M KOH	NF	186 mV@10 mA cm^{-2}	98	N/A
IFP-8 [83]	1 M KOH	NF	319 mV@10 mA cm^{-2}	64	13 h@10 mA cm^{-2}
Fe-MOFs@Ni-MOFs [84]	1 M KOH	CP	275 mV@10 mA cm^{-2}	56.7	100 h@1.52 V *vs.* RHE
Fe-Co-Ni MOF [85]	1 M KOH	NF	254 mV@10 mA cm^{-2}	51.3	48 h@100 mA cm^{-2}
$Co_{0.6}Fe_{0.4}$-MOF-74 [92]	1 M KOH	RRDE [b)]	280 mV@10 mA cm^{-2}	56	12 h@1.53 V *vs.* RHE
c/*a*-NiFe-MOF [93]	1 M KOH	GCE	236 mV@10 mA cm^{-2}	30	Maintaining at 23 mA cm^{-2} for 12 h
NNU-23 [95]	0.1 M KOH	CC	365 mV@10 mA cm^{-2}	77.2	15 h@1.595 V *vs.* RHE
$A_{2.7}$B-MOF-$FeCo_{1.6}$ [96]	1 M KOH	GCE	288 mV@10 mA cm^{-2}	39	10 h@10 mA cm^{-2}
NiFe-GA [98]	1 M KOH	CP	185 mV@10 mA cm^{-2}	28.74	60 h@10 and 100 mA cm^{-2}
Fe/$Ni_{2.4}$/$Co_{0.4}$-MIL-53 [100]	1 M KOH	GCE	236 mV@20 mA cm^{-2}	53.5	N/A
NiCoFe–NDA [102]	1 M KOH	NF	215 mV@10 mA cm^{-2}	64.1	50 h@100 mA cm^{-2}
$(Ni_2Co_1)_{0.925}Fe_{0.075}$-MOF [103]	1 M KOH	NF	257 mV@10 mA cm^{-2}	41.3	35 h@1.488 V *vs.* RHE
$CoMnLa_{0.2}$-MOF [105]	1 M KOH	Cu foam	201 mV@10 mA cm^{-2}	95	25 h@0.55 V *vs.* Ag/AgCl
FeCo-MNS-1.0 [107]	0.1 M KOH	GCE	298 mV@10 mA cm^{-2}	21.6	N/A
NiCo-UMOFNs [109]	1 M KOH	GCE	250 mV@10 mA cm^{-2}	42	200 h@1.48 V *vs.* RHE
Fe:2D-Co-NS [110]	0.1 M KOH	NF	211 mV@10 mA cm^{-2}	46	96 h@10 mA cm^{-2}
M-PCBN [112]	1 M KOH	CC	232 mV@10 mA cm^{-2}	32	60 h@0.538 V *vs.* Hg/HgO
NiFe-MOF-BF_4^--0.3 [113]	1 M KOH	GCE	237 mV@10 mA cm^{-2}	41	14 h@10 mA cm^{-2}
$[Co_3(HHTP)_2)_4$ [116]	0.1 M KOH	RDE	470 mV@64.64 A mg^{-1}	83	30,000 s@1.7 V *vs.* RHE
NiPc-Ni [125]	1 M KOH	GCE	319 mV@10 mA cm^{-2}	83	N/A
3D-Co/NiMOFs [132]	0.1 M KOH	Fe foam	264 mV@10 mA cm^{-2}	54.3	4,000 min@10 mA cm^{-2}
4.3%-NiFe-MOF [136]	0.1 M KOH	NF	~210 mV@ 200 mA cm^{-2}	68	200 h@200 mA cm^{-2}
FeNi MOFs [136]	1 M KOH	NF	239 mV@50 mA cm^{-2}	52.4	1,033 h@100 mA cm^{-2}
SiW_9Co_3[h]@ZIF-67 [149]	0.1 M KOH	RDE	420 mV@10 mA cm^{-2}	93.9	12 h@1.7 V *vs.* RHE

a) PBS means phosphate buffer solution; b) RRDE means rotating ring disk electrode.

hamper further enhancement of the electrocatalytic properties.

4.2 Mixed-metallic MOFs

Metal doping for the preparation of mixed-metallic MOFs is a hot topic in electrocatalysis applications in recent years [88,89]. The common mixed-metallic MOFs can be binary and ternary metallic MOFs, which are synthesized using transition metals of Fe, Co, Ni, Cu, Mn, Mo, W, V, *etc*. Some high entropy MOFs with five or more metal sources have also gained attention as water splitting electrocatalysts [90,91]. To date, quite a few studies about mixed-metallic MOF electrocatalysts for water splitting, especially for OER, have been reported [92–94]. Encouragingly, the synergistic effects among the mixed metals with certain molar ratios can optimize the adsorption of intermediates and modulate the active metal sites. Additionally, multi-metals can efficiently regulate the electronic structures and coordination environments in MOFs, which are favorable to boost the electrocatalytic performance.

For instance, Lan's research group [95] designed a series of stable bimetallic MOFs of $Fe_2M(\mu_3\text{-}O)(CH_3COO)_6(H_2O)_3$ (**NNU-21**–**NNU-24**) containing different Fe_2M (M = Fe, Co, Ni, Zn) cluster nodes (Figure 4a). An iron atom in the Fe_3 nodes could be substituted by a second metal with a similar radius to form the soluble Fe_2M clusters that were favorable for the formation of the desired bimetallic MOFs. **NNU-23** assembled by the Fe_2Ni cluster and the biphenyl-3,4′,5-tricarboxylic acid (BPTC) ligand showed the best electrocatalytic performance among all samples for OER, possessing a η_{10} value of 365 mV, a Tafel slope of 77.2 mV

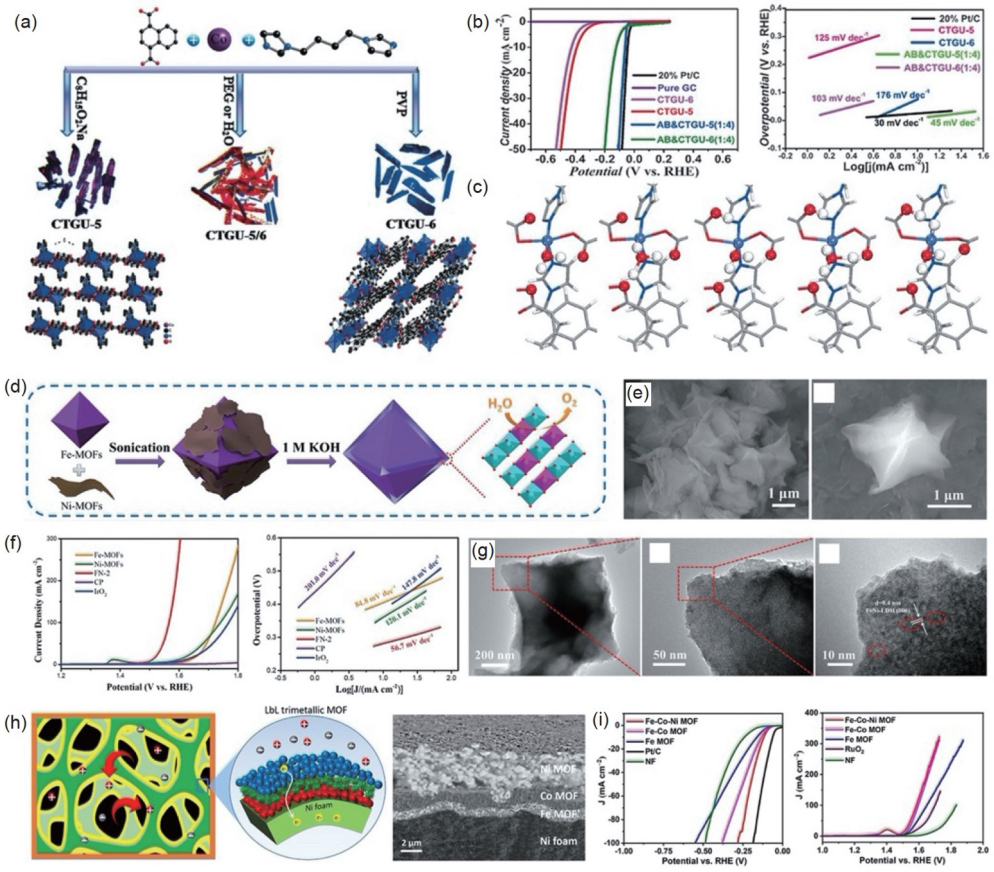

Figure 2 (a) Schematic illustration of two polymorphic Co-MOFs prepared using different surfactants. (b) LSV curves and Tafel plots of AB&CTGU-5 and control samples for HER in 0.5 M H_2SO_4. (c) Possible HER reaction path on the surface of CTGU-5. Reproduced with permission from Ref. [82], copyright 2017 John Wiley & Sons, Inc.. (d) Schematic illustration of Fe-MOFs@Ni-MOFs as OER electrocatalyst. (e) SEM images of Fe-MOFs@Ni-MOFs. (f) LSV curves and Tafel plots of Fe-MOFs@Ni-MOFs and control samples for OER. (g) TEM images of Fe-MOFs@Ni-MOFs with different magnifications after OER stability test. Reproduced with permission from Ref. [84], copyright 2019 John Wiley & Sons, Inc. (h) Schematic illustration of tri-layer Fe-Co-Ni MOF and cross-sectional SEM image. (i) LSV curves of Fe-Co-Ni MOF and control samples for HER and OER. Reproduced with permission from Ref. [85], copyright 2022 American Chemical Society (color online).

dec^{-1}, and a large TOF value of 0.030 s^{-1} at an overpotential of 400 mV in an alkaline solution (Figure 4b). Density functional theory (DFT) calculations revealed that the introduction of a second metal could make the d-band center of Fe_2M clusters closer to Fermi level than that of the Fe_3 cluster, thereby enabling stronger adsorption to reaction intermediates (Figure 4c). Xue *et al*. [96] designed a bimetallic MOF of $A_{2.7}$B-MOF-$FeCo_{1.6}$, which was assembled by two metals of Fe/Co and mixed ligands of terephthalic acid (A) and 2-aminoterephthalic acid (B) (Figure 4d). The structure of $A_{2.7}$B-MOF-$FeCo_{1.6}$ was the same as the typical MIL-88B-Fe MOF, in which Fe^{3+} and terephthalic acid are partially replaced by Co^{2+} and 2-aminoterephthalic acid, respectively. $A_{2.7}$B-MOF-$FeCo_{1.6}$ demonstrated enhanced OER activity with a η_{10} value of 288 mV and a small Tafel slope of 39 mV dec^{-1} due to the optimized electronic structures by modifying its mixed metal nodes and organic linkers. The introduction of Co ions could increase many electrons in the 3d orbital, facilitating the formation of OOH intermediates to further promote its OER activity (Figure 4e).

Dong's research group [97] prepared bimetallic MOF nanosheet arrays (CoNi-MOFNA) *in situ* on a CoNi alloy foam substrate using a self-dissociation-assembly method (Figure 4f). The CoNi foam directly provided bimetallic sources for the nucleation and growth of CoNi-MOFNA homogeneously. Remarkably, Co_9Ni_1-MOFNA with an optimized Co/Ni molar ratio demonstrated excellent electrocatalytic activity for OER with a low η_{10} value of 215 mV and long-term stability over 300 h owing to the defected CoO_5/NiO_5 metal sites and electronic interactions. The time-dependent X-ray absorption fine structure (XAFS) studies found that the small-sized metal oxyhydroxide species were formed on the surface of the catalyst during the OER process (Figure 4g). In 2022, Fang *et al*. [98] synthesized a bioinspired NiFe-gallate MOF (NiFe-GA) with hexagonal prism-shaped structures using Ni^{2+}/Fe^{2+} as metal sources and gallic acid (GA) as ligands. They found that the bimetal nodes were active sites while Fe and GA could promote the formation of active oxygen species for OER. Zhu and co-workers [99]

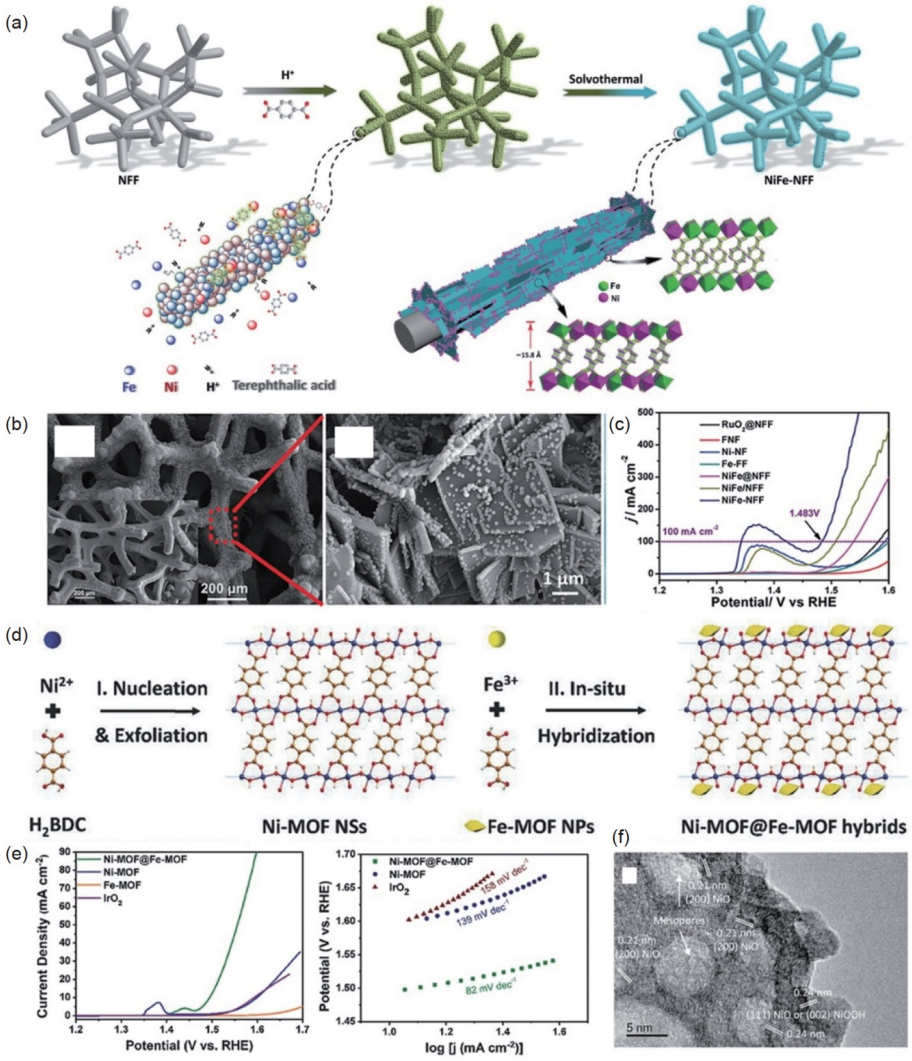

Figure 3 (a) Schematic illustration of the preparation of NiFe-NFF. (b) SEM images of NiFe-NFF. (c) LSV curves of NiFe-NFF and control samples for OER. Reproduced with permission from Ref. [86], copyright 2019 John Wiley & Sons, Inc. (d) Schematic illustration of the synthesis of Ni-MOF@Fe-MOF. (e) LSV curves and Tafel plots of Ni-MOF@Fe-MOF and control samples for OER. (f) HRTEM image of Ni-MOF@Fe-MOF after the OER test. Reproduced with permission from Ref. [87], copyright 2018 John Wiley & Sons, Inc. (color online).

reported a 3D cationic NiFe-azolate MOF (NiFe-btz) film grown on an NF substrate using a semisacrificial template method, which was assembled with azolate ligands and Ni $(OH)_2$ layer as metal sources. The as-prepared NiFe-btz/NF-OH was applied as the working electrode to achieve an enhanced OER performance with a low η_{10} value of 239 mV and a Tafel slope of 44.3 mV dec^{-1} due to its ionic structures and abundant active sites. According to DFT calculations, XPS, and *in situ* Raman investigations, the coupling effect between Ni and Fe ions could promote the charge transfer efficiently, and the formation of MOOH intermediates during OER ensured its electrocatalytic stability.

Compared with bimetallic MOF electrocatalysts, trimetallic MOFs are likely to possess more active metal sites and modulated electronic structures, demonstrating more potential as excellent catalysts for water splitting [100,101]. In 2021, Yue *et al*. [102] reported a 2D trimetallic MOF (Ni-CoFe-NDA) as an efficient OER electrocatalyst. NiCoFe-NDA was assembled by three 3d metals of Fe/Co/Ni and 2,6-naphthalenedicarboxylic acid (NDA) linker and grown on an NF support through a simple anion exchange method (Figure 5a). Verified by XPS and EXAFS characterizations, the trimetallic nodes in the NiCoFe-NDA MOF had a low coordination number. NiCoFe-NDA exhibited an ultralow η_{10} value of 215 mV, a small Tafel slope of 64.1 mV dec^{-1}, and long-term stability over 50 h in an alkaline solution (Figure 5b). The *in situ* Raman along with TEM and XRD characterizations suggested that the transformed oxyhydroxides were formed as the active sites during the OER electrocatalysis process. The metal oxyhydroxide species contained plenty of unsaturated coordinated environments, thereby offering multi-metallic synergistic effects to boost the OER

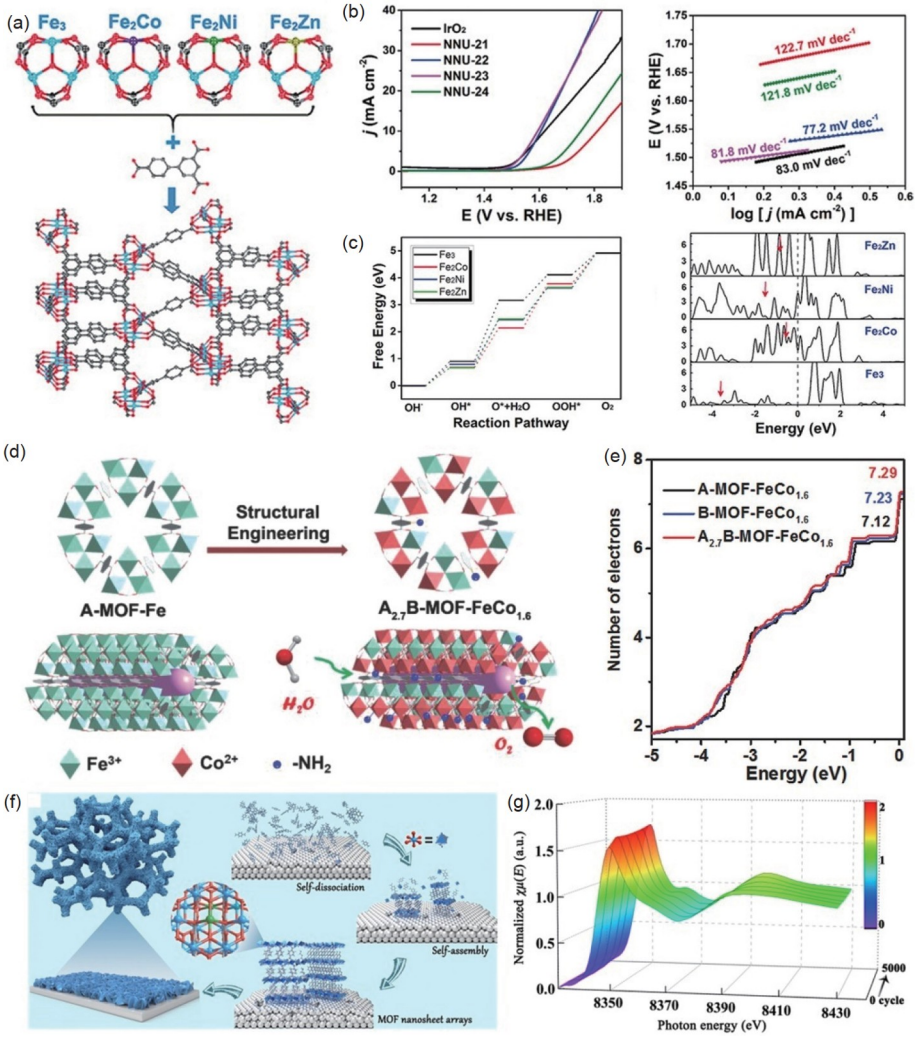

Figure 4 (a) 3D frameworks of **NNU-21**–**NNU-24** assembled by Fe_2M clusters and BPTC ligands. (b) LSV curves and corresponding Tafel plots of **NNU-21**–**NNU-24** and commercial IrO_2 for OER. (c) Free energy diagram of OER on Fe_2M clusters and its projected density of states. Reproduced with permission from Ref. [95], copyright 2018 John Wiley & Sons, Inc. (d) Structures of $A_{2.7}B$-MOF-$FeCo_{1.6}$ with mixed metal nodes and linkers as OER electrocatalyst. (e) Number of 3d electrons in Co. Reproduced with permission from Ref. [96], copyright 2018 John Wiley & Sons, Inc. (f) Schematic illustration of the preparation of CoNi-MOFNA. (g) Ni XANES spectra of CoNi-MOFNA obtained at different CV cycles. Reproduced with permission from Ref. [97], copyright 2020 Elsevier B.V (color online).

performance. Zhang's research group [103] reported a room temperature synthesis strategy to prepare a trimetallic Ni-CoFe-MOF with foam-like structures using three acetates as metal sources and 1,4-BDC as organic ligands (Figure 5c, d). The $(Ni_2Co_1)_{0.925}Fe_{0.075}$-MOF-NF with an optimized metal ratio possessed an extraordinary performance for OER in an alkaline medium, achieving a low η_{10} value of 257 mV and a Tafel slope of 41.3 mV dec^{-1}. According to physical characterizations, the trimetallic MOF nanofoams were oxidation-transformed to metal hydroxides/oxyhydroxides after stability measurement, which were identified as real active species. Han *et al*. [104] reported a 3D trimetallic NiVFe-MOF on NF using a typical solvothermal method. The NiVFe-MOF contained both nanowire and nanosheet morphologies that were favorable for the exposure of active sites and mass transfer for OER.

Doping rare earth metals into multi-metallic MOFs is also a feasible strategy to improve the electrocatalytic efficiency. Wang *et al*. [105] proposed a one-pot solvothermal method to construct a trimetallic $CoMnLa_x$-MOF on Cu foam. The introduction of La to $CoMnLa_x$-MOF could form heterojunction structures with flower-like/flower-bud morphologies, as proved by XRD, TEM, and XPS characterizations. $CoMnLa_x$-MOF with an La/Co/Mn molar ratio of 0.2/1/1 showed an enhanced OER performance, possessing a η_{10} value of 201 mV, a Tafel slope of 95 mV dec^{-1}, and long-term durability over 25 h. Such a heterojunction between CoMn-MOF and La-MOF could optimize the electronic structure and promote the electron/mass transfer during the electrocatalytic process. Recently, Jin and Zhang *et al*. [106] reported trimetallic MOF nanosheet arrays on NF doped with two rare earth elements of Y and Ce (NiYCe-MOF/NF) *via* a hydrothermal

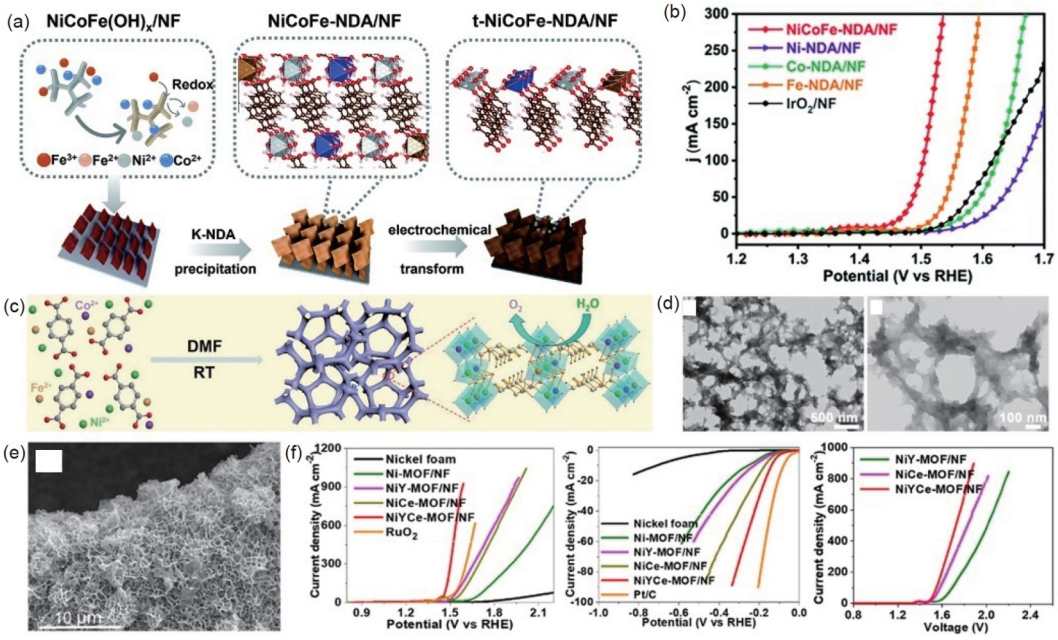

Figure 5 (a) Schematic illustration of the preparation and phase transformation of NiCoFe-NDA. (b) LSV curves of NiCoFe-NDA and control samples for OER. Reproduced with permission from Ref. [102], copyright 2021 Royal Society of Chemistry. (c) Schematic illustration of the synthesis of NiCoFe-MOF nanofoams at room temperature. (d) TEM images of $(Ni_2Co_1)_{0.925}Fe_{0.075}$-MOF-NF. Reproduced with permission from Ref. [103], copyright 2019 John Wiley & Sons, Inc. (e) SEM image of NiYCe-MOF on NF. (f) LSV curves of NiYCe-MOF and control samples for OER, HER, and overall water splitting. Reproduced with permission from Ref. [106], copyright 2022 American Chemical Society (color online).

synthesis method (Figure 5e). The co-doping of Y and Ce in NiYCe-MOF with a regulated molar ratio could modify the electronic structure and accelerate the electron transfer to the Ni sites effectively. NiYCe-MOF/NF showed superior electrocatalytic activities for HER, OER, and overall water splitting in an alkaline electrolyte (Figure 5f).

Consequently, introducing other metals to modulate and activate the pristine metal centers in mixed-metallic MOFs is a significant and promising strategy to improve the electrocatalytic performance for HER and OER.

4.3 MOF nanosheets

In addition to the enhancement of electrocatalytic performance by adjusting the mixed metals in MOFs, morphology control has also been studied to improve their activities. Significantly, MOF nanosheets have emerged as prospective electrocatalysts because the ultrathin nanosheet morphology can expose considerable active metal sites, form coordinatively unsaturated sites, and increase electrical conductivities for desirable water splitting performance [42,107,108].

For example, Tang and co-workers [109] synthesized NiCo bimetal-organic framework nanosheets (NiCo-UMOFNs) using a top-down method by ultrasonicating an MOF colloidal suspension under an airtight condition. Due to the existence of the coordinatively unsaturated metal sites and the synergistic effect between Ni and Co, NiCo-UMOFNs loaded on the glassy-carbon electrode showed improved electrocatalytic OER activity with a η_{10} value of 250 mV and a Tafel slope of 42 mV dec^{-1} in 1 M KOH. Zhang's research group [110] utilized an electrochemical exfoliation strategy to prepare 2D MOF nanosheets from a novel pillared-layer MOF (Figure 6a). The 3D pillared-layer MOF of $(H_3O)_2[Co_6O(dhbdc)_2(H_2dhbdc)_2(EtOH)_4]\cdot 2EtOH$ (**3D-Co**) was hydrothermally synthesized using raw materials of $Co(CH_3COO)_2$ and 2,3-dihydroxy-1,4-benzenedicarboxylic acid (H_4dhbdc) ligand (Figure 6b). When **3D-Co** was grown on a Co film as a working electrode for OER, it was electrochemically transformed to ultrathin nanosheets (**2D-Co-NS**) with a thickness of ~2 nm. Remarkably, Fe-doped **2D-Co-NS** on NF oxidation-transformed from **3D-Co@Ni** before being immersed in the $FeSO_4$ solution demonstrated an ultralow η_{10} value of 211 mV, a small Tafel slope of 46 mV dec^{-1}, and long-term stability of 96 h for OER (Figure 6c). Zhu and co-workers [111] described an LDHs-assisted strategy for the synthesis of 2D bimetallic NiFe MOF nanosheets (NiFe-2D MOF NSs) by the coordination of BDC ligands and LDH precursors using a solvothermal approach. The LDH precursor ensured the as-formed NiFe MOF have bimetallic species and abundant active sites. Moreover, the acidic BDC ligands could controllably transfer metal sources from LDH to MOF, making the as-formed NiFe MOF have 2D nanosheet structures. Remarkably, NiFe-2D MOF NSs loaded on a glassy-carbon electrode exhibited a η_{10} value of 260 mV and a Tafel slope of

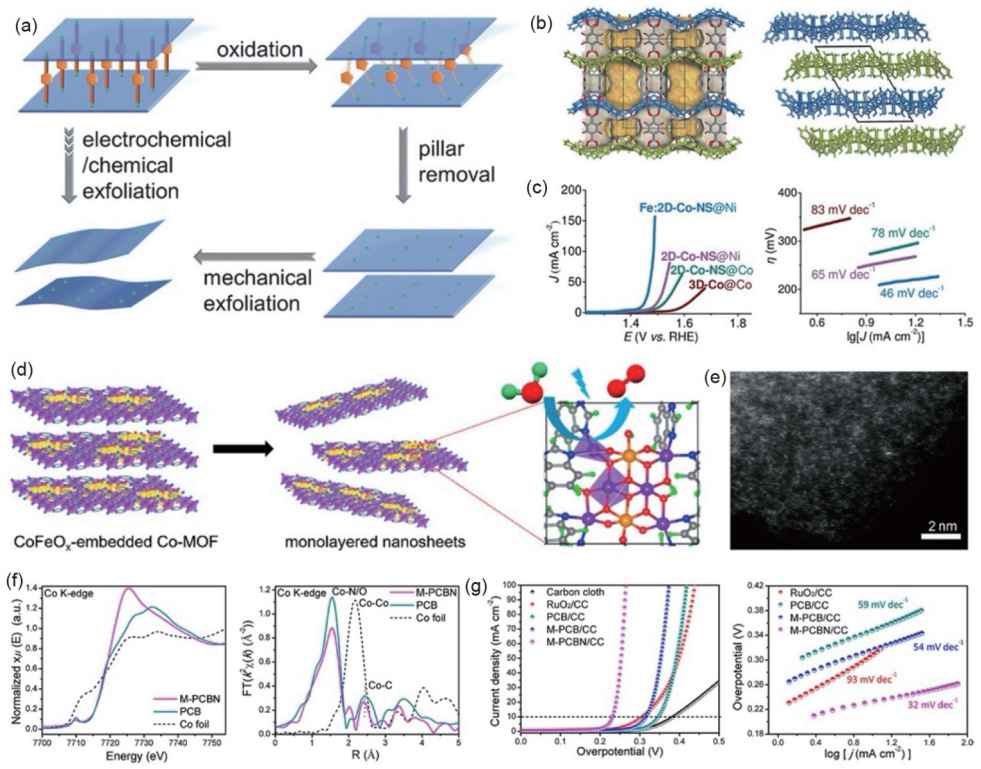

Figure 6 (a) Schematic illustration of the exfoliation of a pillared-layer MOF. (b) 3D pillared-layer MOF structure of **3D-Co** viewed along *a*-axis (left) and 3D packing structure of **2D-Co** viewed along *b*-axis (right). (c) LSV curves and corresponding Tafel plots of Fe-doped **2D-Co-NS** on NF and control samples for OER measured in 0.1 M KOH. Reproduced with permission from Ref. [110], copyright 2018 John Wiley & Sons, Inc. (d) Schematic illustration of the exfoliation of M-PCBN. (e) XANES curves and EXAFS $k^2\chi(k)$ FT spectrum of M-PCBN. (f) HAADF-STEM image of M-PCBN. (g) LSV curves and corresponding Tafel plots of M-PCBN and control samples for OER. Reproduced with permission from Ref. [112], copyright 2020 American Chemical Society (color online).

56 mV dec^{-1} in 1 M KOH. The BDC ligands could provide surface COO^- functional groups, leading to fast proton transfer and OH intermediate adsorption during the OER test.

Introducing small molecules into MOF nanosheets can further optimize their electronic structures. Recently, Zhou and co-workers [112] synthesized CoN_4-based MOF monolayered nanosheets (thickness was ~1 nm) embedded with ultrafine $CoFeO_x$ nanoparticles (M-PCBN) through a facile ultrasonic method (Figure 6d). Aberration-corrected scanning TEM with high-angle annular dark field (HAADF-STEM) and XAS characterizations revealed that plenty of active metal Co sites with higher valences and changed 3d electronic configurations were formed at the interface between $CoFeO_x$ and MOF (Figure 6e, f). DFT calculations further proved that the interfacial CoO_2N_2 sites in M-PCBN ensured the superior OER performance. The as-prepared M-PCBN nanosheets loaded on carbon cloth (CC) achieved a remarkable electrocatalytic performance for OER, possessing a η_{10} value of 232 mV, a small Tafel slope of 32 mV dec^{-1}, as well as good stability over 60 h (Figure 6g). Lang and Niu *et al*. [113] synthesized Ni-based MOF nanosheets with Fe^{3+} ions and BF_4^- anions interspersed between the layers (NiFe-MOF-BF_4^- NSs). The electronic structures could be tailored by the interaction between Ni/Fe ions and BF_4^-, thus optimizing the oxygen intermediates and lowering the free energy barrier to boost the OER activity. The obtained NiFe-MOF-BF_4^--0.3 nanosheets showed outstanding OER electrocatalytic activity due to the M···F interactions, which achieved a η_{10} value of 237 mV and a Tafel slope of 41 mV dec^{-1} in an alkaline solution. Huang and co-workers [114] described a 2D conductive MXene-CoBDC hybrid using $Ti_3C_2T_x$ nanosheets as precursors for the decoration of CoBDC MOF on the surface. The as-form active $Ti_3C_2T_x$-MOF interfaces could facilitate charge transfer and electrolyte contact efficiently, thereby improving its electrocatalytic activity obviously.

As a result, the ultrathin nanosheet structures of MOF electrocatalysts contribute to their exposed metal sites and high electrocatalytic performance for water splitting in most cases. Moreover, the electronic structures of MOF nanosheets can be engineered by some imported small molecules for higher activity and durability.

4.4 Electrically conductive MOFs

It is well known that one of the major problems of MOF electrocatalysts is their poor electrical conducting property.

This is because the pristine MOF crystals with low conductivities are synthesized using hard metal nodes and inert organic ligands in most cases. Recently, scientific researchers have tried to improve MOFs' electrical conductivities for the facilitation of electron transport pathways although they cannot be comparable to those of the typical nano-catalysts [115–118]. Importantly, assembling MOFs through π-conjugated coordination can increase conductivities, thereby making rapid charge transfer to boost their electrocatalytic performance for water splitting [119,120]. The highly delocalized conjugated organic ligands, such as 2,3,6,7,10,11-hexaiminotriphenylene (HITP), are usually chosen to construct MOFs with good electrical conductivities for efficient electrocatalytic investigations [121].

Since the first conductive MOF of $Cu[Cu(pdt)_2]$ was synthesized by Takaishi *et al*. [122] in 2009, conductive MOFs have raised their rapid development in electrochemical catalysis. For example, Huang *et al*. [123] reported three copper(II) benzenehexathiol (Cu-BHT) coordination polymers with different morphologies including thin film, nanocrystal, and amorphous nanoparticle (Figure 7a). Cu-BHT with thin film morphologies showed a higher electrical conductivity of ~1,580 S cm^{-1} than those with nanocrystals (280 S cm^{-1}) and nanoparticles (48 S cm^{-1}). When serving as electrocatalysts for HER at pH 0.0, the Cu-BHT amorphous nanoparticle demonstrated a lower η_{10} value of 450 mV, a smaller Tafel slope of ~95 mV dec^{-1}, and good stability than other Cu-BHT MOFs with different morphologies (Figure 7b). Remarkably, the existence of "Cu-edge" site on the (100) surface was investigated as the exposed active site according to the ΔG_{H^*} energies calculated by DFT simulations. Zhang and colleagues [67] utilized a conjugated ligand of hexaiminohexaazatrinaphthalene (HAHATN) to construct a new 2D bimetallic MOF ($M2_3(M1_3{\cdot}HAHATN)_2$). The conductive $M2_3(M1_3{\cdot}HAHATN)_2$ MOF had a full π-conjugated structure, which was assembled by two transition metals and conjugated organic ligands *via* M-N_4 linkages (Figure 7c). The unsaturated M-N_2 coordination moiety in $M2_3(M1_3{\cdot}HAHATN)_2$ had better activity than that of the M-N_4 linkage, which was favorable for fast electron transfer during the electrocatalysis process. Additionally, the narrow bandgap and electrical conductivity of this conductive MOF were calculated to be 0.19 eV and 2 S cm^{-2}, respectively (Figure 7d). Combined with the above-mentioned advantages, the optimized $Ni_3(Ni_3{\cdot}HAHATN)_2$ nanosheets possessed a η_{10} value of 115 mV and a Tafel slope of 45.6 mV dec^{-1} in an alkaline medium for HER (Figure 7e).

Du's research group [124] synthesized a 2D π-conjugated MOF (NiPc-MOF) using 2,3,9,10,16,17,23,24-octa-aminophthalocyaninato nickel(II) (NiPc-NH_2) as building blocks for the first time. The NiPc-MOF thin film deposited on fluorine-doped tin oxide (FTO) achieved enhanced electrocatalytic performance for OER with an onset potential of 1.48 V *vs*. RHE and a high TOF value of 2.5 s^{-1}. Similarly, in 2021, Li *et al*. [125] reported a series of conductive MOF (MPc-M′) with dual metal sites, which were synthesized using M-phthalocyanine as organic ligands and metal ions *via* square-planar M-O_4 linkages (Figure 7f). DFT calculations suggested that the NiPc-Ni′ MOF had a narrow bandgap and both Ni-N_4 and Ni-O_4 active sites, suggesting its good electrical conductivity. The introduction of extra metals could optimize the d-band center of metal sites to adsorb the oxygen intermediates. Due to the synergistic interaction between Ni-N_4 and Ni-O_4 sites and tailored electronic structures, NiPc-Ni showed improved activity for OER with a η_{10} value of 319 mV and a Tafel slope of 83 mV dec^{-1} in an alkaline medium. Additionally, Wang and Fu *et al*. [126] synthesized π-d-conjugated conductive cobalt-hexaaminobenzene MOF nanosheets (Co-HAB-NSs), which showed good OER activity with a η_{10} value of 310 mV and a small Tafel slope of 56 mV dec^{-1} in 1 M KOH. Shi *et al*. [127] reported a series of conductive $M_3(HHTP)_2$ MOFs using three metals as nodes coordinated to the 2,3,6,7,10,11-hexahydroxytriphenylene (HHTP) ligands. Remarkably, the as-prepared trimetallic MOF of $FeCo_{0.6}Ni_{0.4}$-CAT achieved a low η_{10} value of 277 mV and was transformed to the active oxyhydroxide species during the OER process.

Therefore, a well-designed conjugated structure in MOF electrocatalysts can improve electrical conductivity and facilitate electron transfer for water splitting. In addition, some feasible strategies, such as hybridization with conductive carbon materials [128] and pyrolysis of MOFs [129], have also been widely studied to enhance conductivities of the MOF-based electrocatalysts. Since our review focuses on the discussions of pristine MOF catalysts, the MOF-based composites and derivatives will not be included here.

4.5 MOFs on substrates

In situ growing MOFs on conductive substrates (*e.g*., carbon cloth, carbon fiber paper, Ni foam, Cu foam, Fe foam, and Ti foil) is a practicable strategy to increase conductivity and improve electron transfer ability of MOF electrocatalysts for water splitting. Notably, MOFs on substrates can serve as self-supported working electrodes, demonstrating various array morphologies, such as nanosheets, nanowires, nanorods, and nanoflowers [130,131]. These MOF arrays/substrates possess accessible channels and pores, which are favorable for electrolyte immersion and mass/electron transfer. Furthermore, MOFs grown on substrates can avoid the use of Nafion binder that causes the agglomeration of catalysts and hinders full exposure of the active sites in most cases. The intimate combination of MOFs and substrate can regulate electronic structures for facilitated charge transfer, thereby reducing the electrochemical driving force and

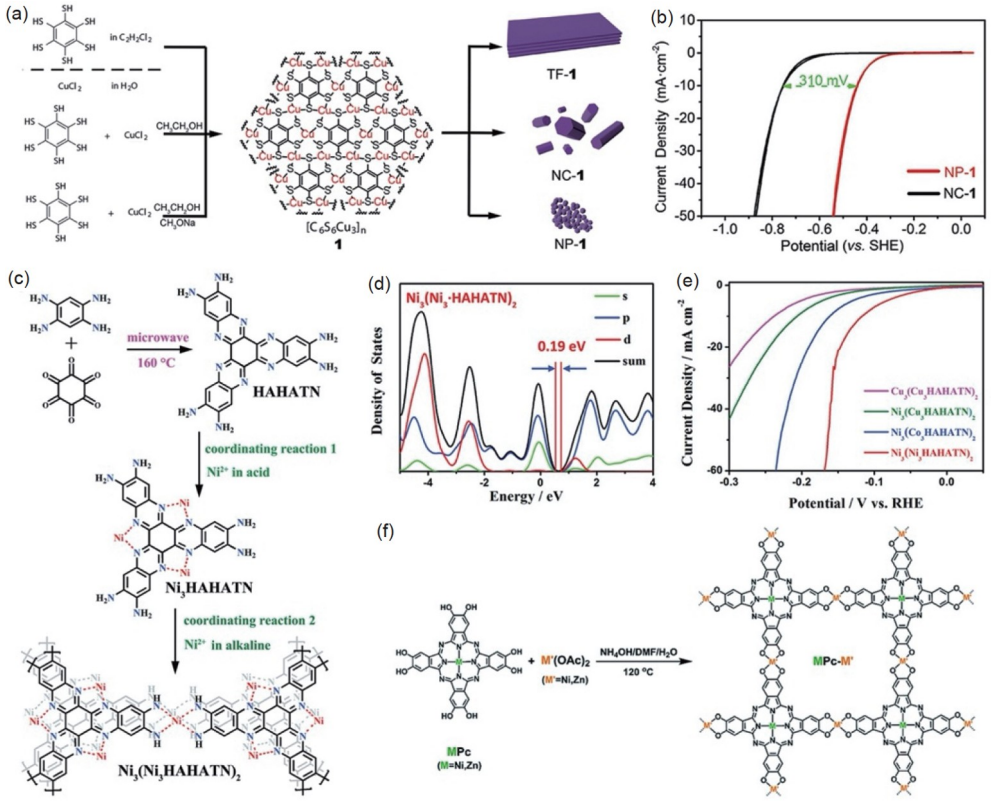

Figure 7 (a) Schematic illustration of the synthesis of Cu-BHT with different morphologies. (b) LSV curves of Cu-BHT with nanocrystal and nanoparticle morphologies for HER in 0.5 M H_2SO_4. Reproduced with permission from Ref. [123], copyright 2009 American Chemical Society. (c) Synthetic scheme of conductive $M2_3(M1_3{\cdot}HAHATN)_2$ MOF. (d) Density of state plot of $Ni_3(Ni_3{\cdot}HAHATN)_2$ by DFT calculations. (e) LSV curves of $Ni_3(Ni_3{\cdot}HAHATN)_2$ and control samples for HER. Reproduced with permission from Ref. [67], copyright 2020 John Wiley & Sons, Inc. (f) Schematic illustration of the preparation of MPc-M′. Reproduced with permission from Ref. [125], copyright 2021 Royal Society of Chemistry (color online).

providing a low energy pathway efficiently. It is worth mentioning that MOFs grown on metal foam substrates can achieve high current density and long-term stability [132]. For instance, NF possesses 3D porous networks, high conductivity, low costs, and active Ni sources, which has been applied for the preparation of MOFs/NF electrodes largely [133,134].

Liu's research group [135] synthesized lattice-strained NiFe MOF nanosheet arrays on an NF substrate using a hydrothermal method coupled with an ultraviolet-light treatment. The π-conjugated naphthalene-based acid ligands were selectively dissociated by ultraviolet irradiation, reducing the interlayer interaction between organic and metal oxide layers and further leading to the enlarged interlayer spacing (Figure 8a). The NiFe MOF with a lattice expansion of 4.3% achieved superior performance for OER than the pristine NiFe MOF, displaying a low overpotential of ~210 mV at a current density of 200 A cm^{-2}, a small Tafel slope of 68 mV dec^{-1}, and excellent durability over 200 h catalyzed at a high current density (Figure 8b). The operando synchrotron spectroscopies of XAS and SR-FTIR characterizations suggested that a key *OOH intermediate was observed on the Ni^{4+} active sites during the OER electrocatalysis process due to the strong Ni–O interaction in the lattice-strained MOFs.

Wang *et al.* [136] reported bimetallic FeNi-MOFs nanoarrays *in situ* grown on NF using Fe^{2+}/Ni^{2+} ions as metal nodes and thiophenedicarboxylate acid (H_2TDC) as organic ligands (Figure 8c). The FeNi-MOFs nanobelts exhibited stable structures immersed in 1 M KOH because the saturated oxygen atoms in the H_2TDC ligands were difficult to attack the OH^- ions. The increased valence of Fe^{3+} ions in the FeNi-MOFs induced a continuous enhancement of electrocatalytic performance for OER, leading to a low overpotential of 239 mV at 50 mA cm^{-2}, a Tafel slope of 52.4 mV dec^{-1}, and long-term durability over 1,033 h operated at a high current density of 100 mA cm^{-2} (Figure 8d). Theoretical calculations suggested that the strong Fe–O bond facilitated the proton/electron transfer and the high active Fe sites ensured the superior OER performance. Lu's research group [66] reported amino-functionalized and water-stable NH_2-MIL-88B(Fe_2Ni) MOF nanosheets *in situ* grown on NF (NFN-MOF/NF) using 2-aminoterephthalic acid as linkers and Fe/Ni ions as metal sources (Figure 8e). The NF substrate was in favor of the oriented formation of 2D MOF nanosheets, thereby providing abundant exposed active sites. The M_3O metal cluster possessed coordinatively unsaturated metal centers due to the lack of water molecules while the $–NH_2$ in the ligands contributed to the enhancement of the

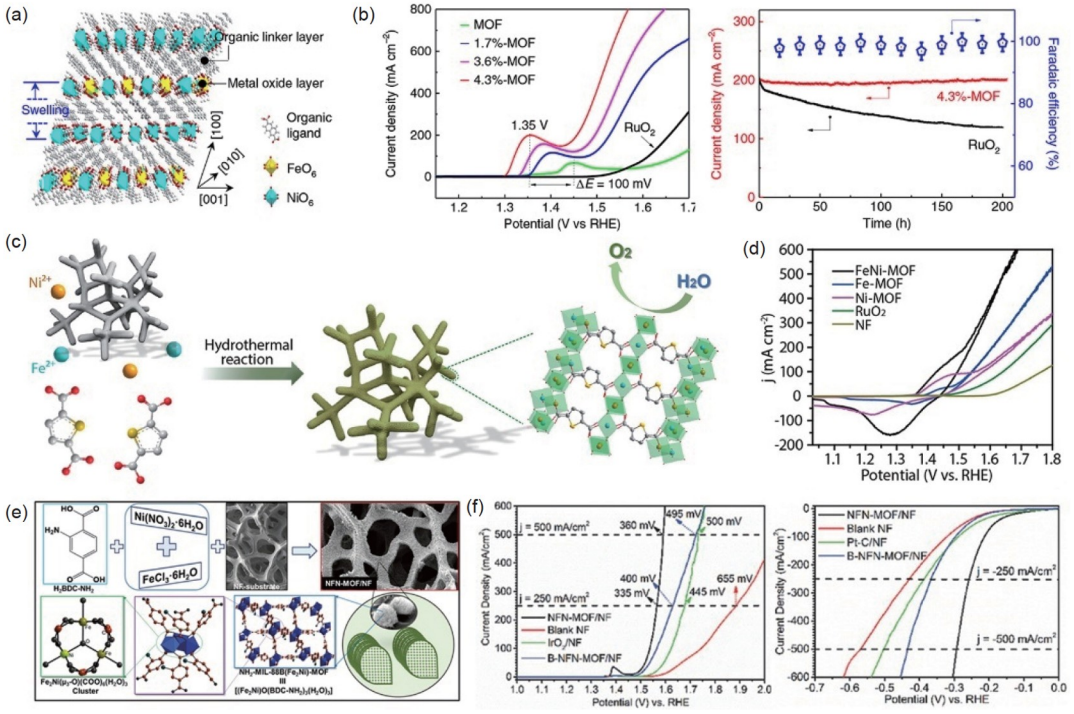

Figure 8 (a) Schematic illustration of structure variation of NiFe MOF on an ultraviolet treatment. (b) LSV and chronoamperometric curves of 4.3%-strained MOFs for OER measured in 0.1 M KOH. Reproduced with permission from Ref. [135], copyright 2019 Springer Nature. (c) Schematic illustration of the preparation of FeNi-MOFs on NF. (d) CV curves of FeNi-MOFs and control samples for OER. Reproduced with permission from Ref. [136], copyright 2021 American Chemical Society. (e) Schematic illustration of the synthesis of NH_2-MIL-88B(Fe_2Ni) MOF nanosheets on NF. (f) LSV curves of NFN-MOF/NF and control samples for OER and HER, respectively. Reproduced with permission from Ref. [66], copyright 2018 John Wiley & Sons, Inc. (color online).

electrocatalytic efficiency. The active $\{Fe_2Ni(\mu_3\text{-}O)(COO)_6(H_2O)_3\}$ cluster and synergistic effects between Fe and Ni as well as MOF and NF enabled its excellent electrocatalytic performance and long-term stability in 1 M KOH, achieving low η_{10} values of 87 and 240 mV for HER and OER, respectively (Figure 8f).

In this respect, MOFs on the NF substrates as working electrodes acquire excellent activity and electrocatalytic stability in a harsh electrolyte. It is noteworthy that other metal foams and carbon-based substrates also have been used to serve as popular conductive substrates for the growth of MOFs. For example, Gu's research group [137] synthesized bimetallic Co/Ni(BDC)$_2$TED MOF thin film arrays *in situ* on Cu foam using a liquid-phase epitaxial layer-by-layer method. During the synthesis process, the Cu foam substrate was sequentially immersed in Co/Ni metal ions and mixed ligands of 1,4-BDC and triethylenediamine (TED) solutions (Figure 9a). The Co/Ni(BDC)$_2$TED MOF showed good orientation and adhesion on Cu foam, possessing many active sites for enhanced OER performance. The optimized Co/Ni(BDC)$_2$TED MOF nanosheets with Co/Ni molar ratio of 1:1 and 40 growth cycles showed a η_{10} value of 287 mV, a Tafel slope of 76.24 mV dec^{-1}, and good electrolysis stability for 25 h (Figure 9b). DFT calculation results revealed that the Ni and Co nodes exhibited high activity for the initial and electron transfer processes for OER, respectively, and combining them considerably reduces the kinetic barriers (Figure 9c). In 2022, Song *et al.* [138] reported oxygen-defected Fe-MOF nanosheet arrays on an iron foam substrate (O_v-Fe MOF/IF) by a plasma-engraving treatment. The O_v-Fe MOF/IF demonstrated superior HER, OER, and overall water splitting performance in an alkaline medium due to its porous structures, unsaturated metal sites, and modified electronic states.

Wang *et al.* [64] proposed a lattice-matching growth method to synthesize a conductive trimetallic MOF/layered double hydroxide nanotube arrays (cMOF/LDH) on a CC substrate (Figure 9d). The CoNiFe-LDH nanowires were formed on CC, which served as the interior template for further growth of cMOF nanotubes *via* coordination bonds. cMOF/LDH exhibited lattice matched core-shell heterostructures to expose more active sites and promote charge transfer helpfully. The as-prepared cMOF/LDH heteronanotube on CC showed improved OER activity with a low overpotential of 216 mV at 50 mA cm^{-2} and a Tafel slope of 34.1 mV dec^{-1} for OER (Figure 9e). Han and Liu *et al.* [62] proposed a general *in situ* transformation of layered double hydroxides precursor strategy to synthesize a series of bimetallic MOFs on three conductive substrates. By changing metal sources and ligands, various bimetallic MOFs on NF, CC, and carbon fiber paper (CFP) could be prepared separately, showing similar morphologies of ultrathin nanosheet

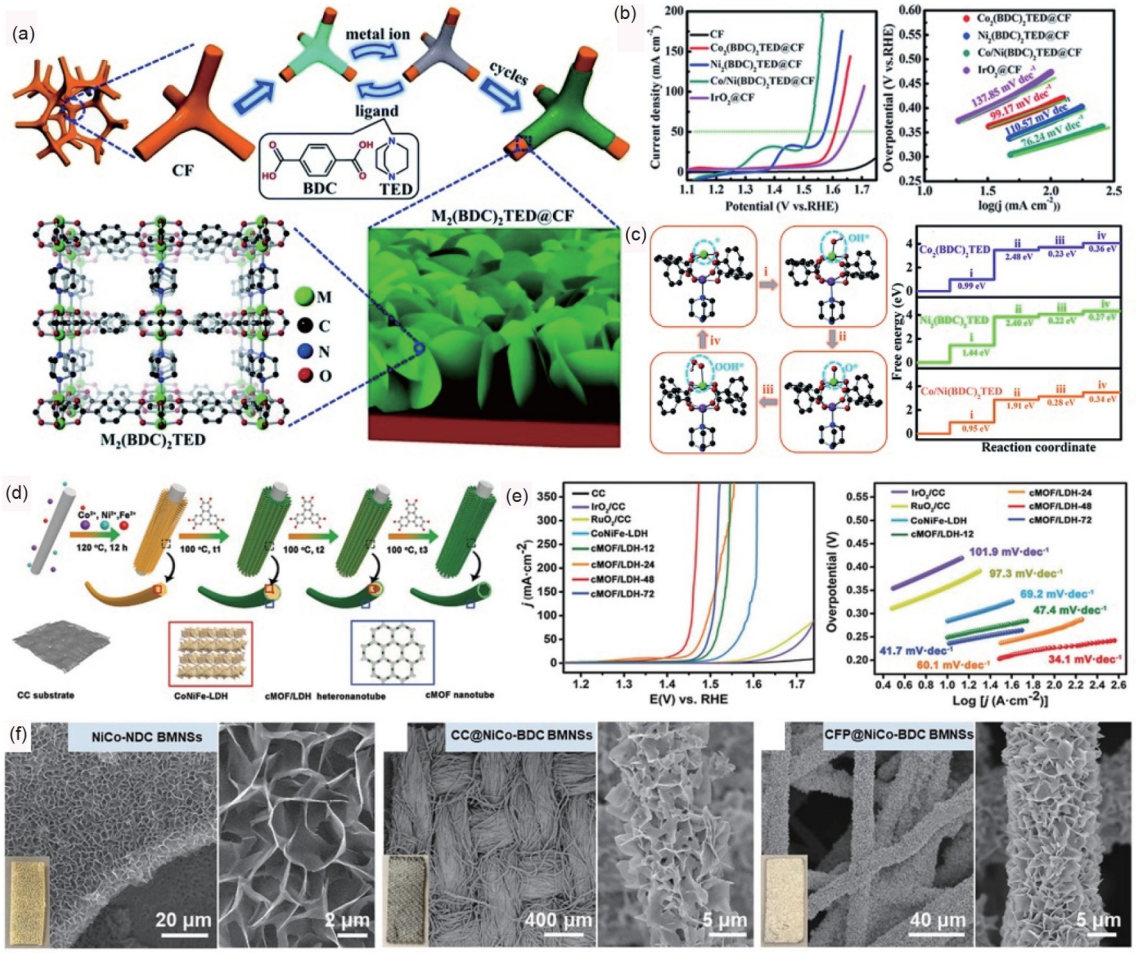

Figure 9 (a) Schematic illustration of the synthesis of Co/Ni(BDC)$_2$TED MOF on Cu foam. (b) LSV curves and corresponding Tafel plots of Co/Ni (BDC)$_2$TED MOF and control samples for OER. (c) DFT calculation results of Co/Ni(BDC)$_2$TED for OER. Reproduced with permission from Ref. [137], copyright 2019 Royal Society of Chemistry. (d) Schematic illustration of the synthesis of cMOF/LDH on CC. (e) LSV curves and corresponding Tafel plots of cMOF/LDH and control samples for OER. Reproduced with permission from Ref. [64], copyright 2021 John Wiley & Sons, Inc. (f) SEM images of bimetallic MOF nanosheets on NF, CC, and CFP substrates, respectively. Reproduced with permission from Ref. [62], copyright 2019 John Wiley & Sons, Inc. (color online).

arrays (Figure 9f). As a direct working electrode, the NiCo-BDC MOF on NF possessed a superior OER performance with a η_{10} value of 230 mV and a small Tafel slope of 61 mV dec^{-1}.

As shown in the above studies, *in situ* growth of MOFs on conductive substrates can not only improve the conductivity and activity for efficient HER and OER performances but also form regular nanoscale MOF arrays to accelerate the charge transfer and high exposure of active sites.

4.6 Polyoxometalate-based MOFs

Although MOFs have many advantages for electrocatalysis applications, the unstable structures and insufficient metal active sites limit their significant performance enhancement. As molecular metal oxide anions, polyoxometalates (POMs) possess diverse topological structures, tailorable sizes, abundant surface oxygen atoms, and reversible electron transfer abilities, which are beneficial for electrochemical applications [139,140]. POMs, especially Mo- and W-based POMs, can be immobilized in well-defined pores or coordinated with ligands of MOFs to form POM-based MOFs (POMOFs) [141]. In many instances, POMOFs demonstrate excellent electrocatalytic activities on account of their ultrastable structures, uniform dispersion of POMs in MOF crystals, and abundant active sites from POMs [142–144].

In 2011, a POMOF of $(TBA)_3[PMo^{V}_{8}Mo^{VI}_{4}O_{36}(OH)_4Zn_4]$-$[C_6H_3(COO)_3]_{4/3}\cdot 6H_2O$ (***ε*(trim)$_{4/3}$**) was reported as the HER electrocatalyst by Doldecq and co-workers [145]. This is the first report using MOFs as direct catalysts for electrocatalytic water splitting. The ***ε*(trim)$_{4/3}$** POMOF showed a 3D open-framework with Keggin POM units connected by trim linkers and filled with tetrabutylammonium (TBA) counterions in channels. The as-prepared ***ε*(trim)$_{4/3}$**/carbon paste electrode exhibited a high hydrogen evolution yield of >95% and a turnover number of 1.2×10^5 in an acid medium (pH = 1).

However, the evaluation parameters for HER were incomplete, and no mechanism analysis was proposed.

Interestingly, Lan and Zhou *et al*. [146] synthesized a new porous POMOF, $[TBA]_3[\varepsilon\text{-}PMo^{V}_{8}Mo^{VI}_{4}O_{36}(OH)_4Zn_4][BTB]_{4/3}\cdot x$Guest (**NENU-500**), using a POM fragment of Zn-ε-Keggin-Cl as nodes connected to BTB^{3-} organic ligands (Figure 10a). Remarkably, **NENU-500** with a unique 3D open framework and **ctn** topology showed good structural stability and strong tolerance in both acidic and basic media (Figure 10b). Taking the advantages of redox activity of the POM fragment and porosity of the MOF framework, **NENU-500** exhibited excellent electrocatalytic activity for HER in an acidic electrolyte, possessing a low η_{10} value of 237 mV, a small Tafel slope of 96 mV dec^{-1}, and maintainable stability activity after 2,000 CV cycles (Figure 10c). DFT calculations using a Zn-ε-Keggin-Cl fragment as a theoretical model found that μ_3-bridging oxygen site had lower adsorption energy than other oxygen sites for H adsorption. Similarly, Wang *et al*. [147] synthesized a ZnMo-POMOF crystal with nanoflower array morphologies on NF recently. The ZnMo-POMOF with a formula of $[\varepsilon\text{-}PMo^{V}_{8}Mo^{VI}_{4}O_{37}(OH)_3Zn_4]\text{-}[BPB]_3$ was constructed using a Keggin-typed POM fragment of $\{\varepsilon\text{-}PMo^{V}_{8}Mo^{VI}_{4}O_{37}Zn_4\}$ as building nodes connected to 1,4-bis(pyrid-4-yl)benzene (BPB) ligands. Due to the active Zn-ε-Keggin polymolybdate units and enhanced conductivity, ZnMo-POMOF on NF could serve as the working electrode for HER, possessing a η_{10} value of 118 mV and a Tafel slope of 66 mV dec^{-1} in an acidic medium.

In addition to serving as inorganic nodes, POMs could be confined within pores or cavities of MOFs to synthesize stable POMOF crystals or POM/MOF materials. In the work reported by Zhang *et al*. [148], two isostructural POM-encapsulated metal-organic nanotube frameworks of $[Cu^{II}_{6}\text{-}(pzta)_6(bpy)_3(X_2W_{18}O_{62})]\cdot 2H_2O$ (**HUST-200**, X = P and **HUST-201**, X = As) were synthesized successfully (Figure 10d). The metal-organic nanotube (MONT) hosts were constructed using Cu ions connected by mixed ligands of 5-(2-pyrazinyl)tetrazole (pzta) and 4,4′-bipyridine (bpy) while the POM cluster was the $[X_2W_{18}O_{62}]^{6-}$ polyanion. The encapsulation of POMs in the pores of the MONTs could increase the chemical stability while their electrocatalytic activities for HER were unaffected. Accordingly, **HUST-200** loaded with 50 wt% carbon black displayed a η_{10} value of 131 mV, a small Tafel slope of 51 mV dec^{-1}, and a high j_0 value of 0.53 mA cm^{-2} for HER in an acidic medium. Besides, Abdelkader-Fernández and co-workers [149] explored the encapsulation of Keggin-typed $SiW_{11}Co$ or SiW_9Co_3 POMs into the cavities of ZIF-67 to prepare the POM@ZIF-67 composites with different POM loadings. Due to their different solubilities in the reaction media, the $SiW_{11}Co$ POMs had a higher loading in ZIF-67 than that of SiW_9Co_3, which were confined within the cages near the surface of ZIF-67 preferentially and homogeneously (Figure 10e). Especially, due to the abundant Co active sites, high POMs loading, and open defect-rich structures, SiW_9Co_3[h]@ZIF-67 showed superior electrocatalytic performance for OER in 0.1 M KOH, achieving a η_{10} value of 420 mV, a Tafel slope of 93.9 mV dec^{-1}, and long-term stability over 12 h. In brief, combining POMs with MOFs could prepare POMOF-based electrocatalysts with excellent structural stability and electrocatalytic activity.

5 Summary and outlooks

Electrocatalytic water splitting is a key and promising technology in energy storage and conversion applications. Designing and preparing low-cost, high-efficient, and robust electrocatalysts is crucial to meeting the requirements of industrial manufacturing. MOFs have been regarded as a new generation of high-efficient electrocatalysts for HER and OER due to their precise structures, periodic pores, large surface areas, regulatable metal nodes, functionalized ligands, and various compositions. In this review, we summarize the rational design and synthesis of MOFs as outstanding electrocatalysts for water splitting. First, design concepts including precise structure modulation, regulation of MOF dimensions, metal nodes/ligands modifications, and structural reconstruction have been analyzed and highlighted to boost the electrocatalytic performance of MOFs. Second, the advantages and disadvantages of three common strategies for the synthesis of activated MOF electrocatalysts are introduced. Then, six types of representative MOF electrocatalysts are classified, and their unique structures and remarkable activities are discussed in detail. Notably, we have found that multi-metallic-based MOFs with 2D nanosheet structures demonstrate enhanced intrinsic electrocatalytic performance for HER or OER due to their good conductivities, adjustable multi-metal nodes as active sites, and ultrathin sheet morphologies.

Although significant progress of MOF electrocatalysts for water splitting has been made in recent years, low conductivities, poor structural stability, and insufficient active sites in most MOFs impede their intensive studies and further improvement in performance. There are some key issues and challenges that still need to be further explored.

(1) Costs of MOFs should be taken into account because a low-cost and high-efficient MOF catalyst is more favorable for commercialization. Some vital factors including nontoxic and abundant raw materials, facile synthetic routes, and high yields also need to be taken into consideration for the potential MOF candidates. To date, several MOFs have been produced in quantity as chemicals by different companies, such as MILs and ZIFs, but their commercial applications are still unavailable. Therefore, it is a key issue that we should design and synthesize MOF electrocatalysts with mass

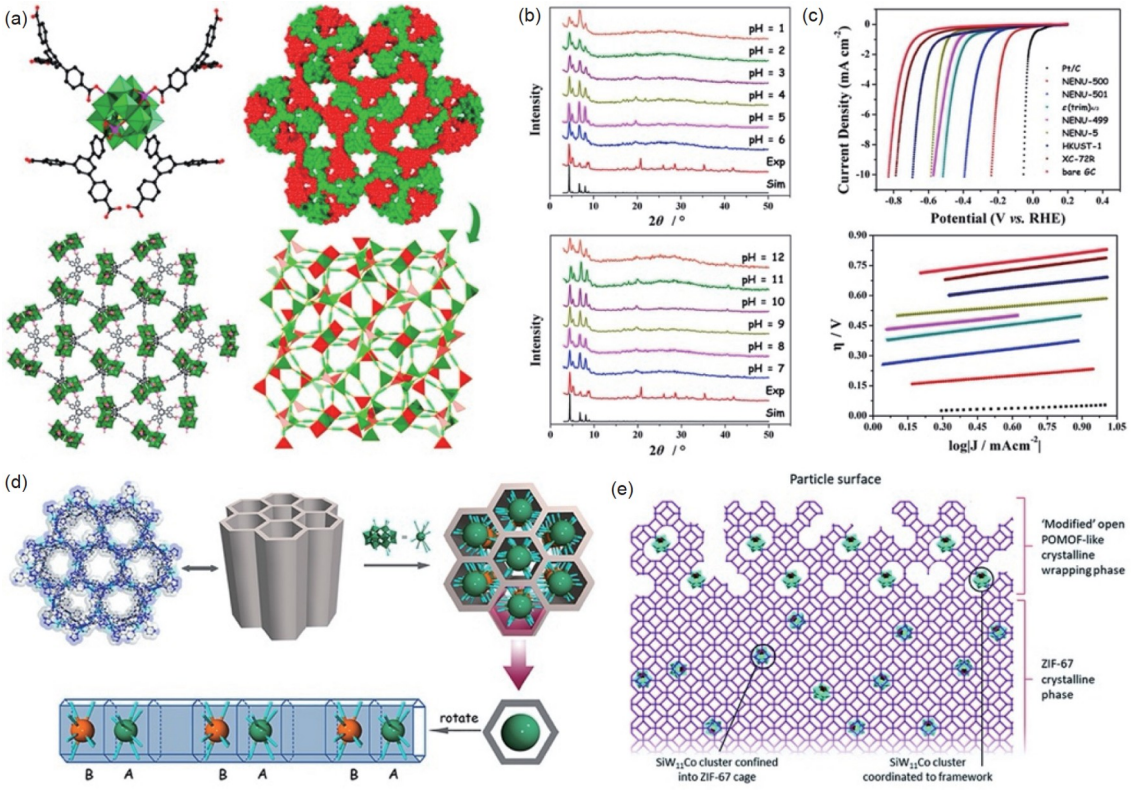

Figure 10 (a) **NENU-500** structures: connection mode between Zn-ε-Keggin and BTB^{3-} ligands, 3D connected framework, and two-fold interpenetrated structures. (b) XRD patterns of **NENU-500** immersed in solutions with different pH values from 1 to 12. (c) LSV curves and corresponding Tafel plots of **NENU-500** and control samples for HER in 0.5 M H_2SO_4. Reproduced with permission from Ref. [146], copyright 2015 American Chemical Society. (d) Schematic illustration of POMs encapsulated within pores of the MONT framework. Reproduced with permission from Ref. [148], copyright 2018 American Chemical Society. (e) Scheme of the proposed structure of $SiW_{11}Co$[h]@ZIF-67. Reproduced with permission from Ref. [149], copyright 2020 Royal Society of Chemistry (color online).

production, high activity, and low cost to meet the demands of industrial applications.

(2) The main disadvantage of poor electrical conductivity for most pristine MOFs limits their usage as direct electrocatalysts. The π-conjugated MOFs assembled with transition metal nodes and aromatic organic ligands have relatively high conductivity but few of them are reported as HER or OER electrocatalysts. To date, many strategies, for instance, pyrolyzing MOFs, growing MOFs *in situ* on conductive supports, and hybridizing MOFs with carbon-based materials or other conductive nanomaterials, have been proposed to improve the activities of MOF-based electrocatalysts. Nevertheless, it is not a universal strategy that works for most MOFs. Hence, designing MOFs with π-conjugated structures and ultrathin 2D structures or modifying their metal nodes/organic ligands show great potential for MOF electrocatalysts. Besides, one main difficulty of easy agglomeration of 2D MOFs should be noticed and solved to obtain highly dispersed 2D MOF nanosheets.

(3) For OER, the structural transformation of MOFs to real active species usually happens during the electrocatalysis process. In some cases, the structural reconstruction process of MOFs is instant, resulting in great difficulties in our studies of the catalytic reactions and mechanisms. Some advanced operando characterization techniques, such as attenuated total reflection infrared (ATR-IR) spectroscopy, Raman spectroscopy, XAS, and scanning probe microscopy, have been applied to gain a deep understanding of the structural transformation for OER. Therefore, it is of great importance that further investigation of MOF electrocatalysts using these new and advanced operando techniques will be helpful to address scientific problems and provide guidance in electrocatalysis applications.

(4) In-depth studies of intrinsic and comprehensive reaction mechanisms of MOF electrocatalysts are urgently needed. It would be meaningful to understand the relationships between structures and properties. Combining advanced operando characterization techniques and theoretical calculations, we hope that intensive research will identify specific electrocatalysis processes and offer available guidance for the design of novel MOF-based electrocatalysts.

Although there are many challenges of MOF electrocatalysts in the electrochemical water splitting fields, the research studies are significant and deserve detailed studies. All in all, we hope this review will help scientific researchers to acquire knowledge of recent developments in MOFs as

excellent electrocatalysts toward HER and OER and provide guidance for the design of high-efficient and inexpensive MOF-based water splitting electrocatalysts to meet the "carbon neutrality" requirements.

Acknowledgements This work was supported by the National Natural Science Foundation of China (22101137), the Natural Science Foundation of Jiangsu Province (BK20210637), and the startup foundation for introducing talent of NUIST (1521622101008).

Conflict of interest The authors declare no conflict of interest.

1 Turner JA. *Science*, 2004, 305: 972–974
2 Chu S, Majumdar A. *Nature*, 2012, 488: 294–303
3 Anantharaj S, Ede SR, Sakthikumar K, Karthick K, Mishra S, Kundu S. *ACS Catal*, 2016, 6: 8069–8097
4 You B, Sun Y. *Acc Chem Res*, 2018, 51: 1571–1580
5 Hu Y, Li F, Long Y, Yang H, Gao L, Long X, Hu H, Xu N, Jin J, Ma J. *J Mater Chem A*, 2018, 6: 10433–10440
6 Yuan F, Liu Y, Ma P, Wang S, Yang G, Qin J, Luo Y, Luo S, Ma. J. *J Colloid Interface Sci*, 2020, 578: 668–676
7 Zeng Y, Zhao M, Huang Z, Zhu W, Zheng J, Jiang Q, Wang Z, Liang H. *Adv Energy Mater*, 2022, 12: 2201713
8 Hu C, Zhang L, Gong J. *Energy Environ Sci*, 2019, 12: 2620–2645
9 Kasian O, Grote JP, Geiger S, Cherevko S, Mayrhofer KJJ. *Angew Chem Int Ed*, 2018, 57: 2488–2491
10 Li Y, Sun Y, Qin Y, Zhang W, Wang L, Luo M, Yang H, Guo S. *Adv Energy Mater*, 2020, 10: 1903120
11 Wu ZP, Lu XF, Zang SQ, Lou XWD. *Adv Funct Mater*, 2020, 30: 1910274
12 Li L, Wang P, Shao Q, Huang X. *Chem Soc Rev*, 2020, 49: 3072–3106
13 Jin M, Zhang X, Niu S, Wang Q, Huang R, Ling R, Huang J, Shi R, Amini A, Cheng C. *ACS Nano*, 2022, 16: 11577–11597
14 Yuan F, Wang S, Liang K, Yang G, Qin J, Gao J, Ma J. *Mol Catal*, 2021, 516: 112006
15 Chen M, Hu Y, Liang K, Zhao Z, Luo Y, Luo S, Ma J. *Nanoscale*, 2021, 13: 18763–18772
16 Wang S, Yuan F, Yang G, Luo S, Chen M, Fan T, Ma J. *Mol Catal*, 2022, 525: 112339
17 Furukawa H, Cordova KE, O'Keeffe M, Yaghi OM. *Science*, 2013, 341: 1230444
18 Zhou HCJ, Kitagawa S. *Chem Soc Rev*, 2014, 43: 5415–5418
19 Bavykina A, Kolobov N, Khan IS, Bau JA, Ramirez A, Gascon J. *Chem Rev*, 2020, 120: 8468–8535
20 Shen Y, Pan T, Wang L, Ren Z, Zhang W, Huo F. *Adv Mater*, 2021, 33: 2007442
21 Dou S, Li X, Wang X. *ACS Mater Lett*, 2020, 2: 1251–1267
22 Dhakshinamoorthy A, Li Z, Garcia H. *Chem Soc Rev*, 2018, 47: 8134–8172
23 Gao J, Huang Q, Wu Y, Lan YQ, Chen B. *Adv Energy Sustain Res*, 2021, 2: 2100033
24 Li J, Bhatt PM, Li J, Eddaoudi M, Liu Y. *Adv Mater*, 2020, 32: 2002563
25 Feng Y, Wang Y, Ying Y. *Coord Chem Rev*, 2021, 446: 214102
26 Lawson HD, Walton SP, Chan C. *ACS Appl Mater Interfaces*, 2021, 13: 7004–7020
27 Li XM, Wang Y, Mu Y, Liu J, Zeng L, Lan YQ. *ACS Appl Mater Interfaces*, 2022, 14: 9264–9271
28 Wang S, Hou Y, Lin S, Wang X. *Nanoscale*, 2014, 6: 9930–9934
29 Qiu T, Liang Z, Guo W, Tabassum H, Gao S, Zou R. *ACS Energy Lett*, 2020, 5: 520–532
30 Yin Z, Liang J, Zhang ZY, Luo H, Zhou J. *J Colloid Interface Sci*, 2022, 623: 405–416
31 Zhang M, Hu D, Xu Z, Liu B, Boubeche M, Chen Z, Wang Y, Luo H, Yan K. *J Mater Sci Tech*, 2021, 72: 172–179
32 Wei YS, Zou L, Wang HF, Wang Y, Xu Q. *Adv Energy Mater*, 2022, 12: 2003970
33 Song XZ, Zhang N, Wang XF, Tan Z. *Mater Today Energy*, 2021, 19: 100597
34 Zhang K, Liang Z, Zou R. *Sci China Chem*, 2020, 63: 7–10
35 Shen JQ, Liao PQ, Zhou DD, He CT, Wu JX, Zhang WX, Zhang JP, Chen XM. *J Am Chem Soc*, 2017, 139: 1778–1781
36 Zhang Z, Gómez-García CJ, Wu Q, Xin J, Pang H, Ma H, Chai D, Li S, Zhao C. *Inorg Chem*, 2022, 61: 11830–11836
37 Noh H, Kung CW, Otake K, Peters AW, Li Z, Liao Y, Gong X, Farha OK, Hupp JT. *ACS Catal*, 2018, 8: 9848–9858
38 Wang M, Xu Y, Peng CK, Chen SY, Lin YG, Hu Z, Sun L, Ding S, Pao CW, Shao Q, Huang X. *J Am Chem Soc*, 2021, 143: 16512–16518
39 Deng L, Hu F, Ma M, Huang SC, Xiong Y, Chen HY, Li L, Peng S. *Angew Chem Int Ed*, 2021, 60: 22276–22282
40 Xiao X, Zou L, Pang H, Xu Q. *Chem Soc Rev*, 2020, 49: 301–331
41 Zhang W, Zhou K. *Small*, 2017, 13: 1700806
42 Zhu D, Qiao M, Liu J, Tao T, Guo C. *J Mater Chem A*, 2020, 8: 8143–8170
43 Duan J, Chen S, Zhao C. *Nat Commun*, 2017, 8: 15341
44 Zhou J, Dou Y, Wu XQ, Zhou A, Shu L, Li JR. *Small*, 2020, 16: 1906564
45 Zhou W, Xue Z, Liu Q, Li Y, Hu J, Li G. *ChemSusChem*, 2020, 13: 5647–5653
46 Gu M, Wang SC, Chen C, Xiong D, Yi FY. *Inorg Chem*, 2020, 59: 6078–6086
47 Xu YT, Ye ZM, Ye JW, Cao LM, Huang RK, Wu JX, Zhou DD, Zhang XF, He CT, Zhang JP, Chen XM. *Angew Chem Int Ed*, 2019, 58: 139–143
48 Feng K, Zhang D, Liu F, Li H, Xu J, Xia Y, Li Y, Lin H, Wang S, Shao M, Kang Z, Zhong J. *Adv Energy Mater*, 2020, 10: 2000184
49 Lu XF, Liao PQ, Wang JW, Wu JX, Chen XW, He CT, Zhang JP, Li GR, Chen XM. *J Am Chem Soc*, 2016, 138: 8336–8339
50 Xue Z, Liu K, Liu Q, Li Y, Li M, Su CY, Ogiwara N, Kobayashi H, Kitagawa H, Liu M, Li G. *Nat Commun*, 2019, 10: 5048
51 He F, Zhao Y, Yang X, Zheng S, Yang B, Li Z, Kuang Y, Zhang Q, Lei L, Qiu M, Dai L, Hou Y. *ACS Nano*, 2022, 16: 9523–9534
52 Tao L, Lin CY, Dou S, Feng S, Chen D, Liu D, Huo J, Xia Z, Wang S. *Nano Energy*, 2017, 41: 417–425
53 Gao Z, Lai Y, Gong L, Zhang L, Xi S, Sun J, Zhang L, Luo F. *ACS Catal*, 2022, 12: 9101–9113
54 Ding M, Cai X, Jiang HL. *Chem Sci*, 2019, 10: 10209–10230
55 Zhao S, Tan C, He CT, An P, Xie F, Jiang S, Zhu Y, Wu KH, Zhang B, Li H, Zhang J, Chen Y, Liu S, Dong J, Tang Z. *Nat Energy*, 2020, 5: 881–890
56 Jiang J, Huang L, Liu X, Ai L. *ACS Appl Mater Interfaces*, 2017, 9: 7193–7201
57 Yang K, Jin Z, Zhang Q, Chen Q, Peng W, Li Y, Zhang F, Xia Q, Fan X. *Chem Commun*, 2022, 58: 1115–1118
58 Sun H, Chen L, Lian Y, Yang W, Lin L, Chen Y, Xu J, Wang D, Yang X, Rümmerli MH, Guo J, Zhong J, Deng Z, Jiao Y, Peng Y, Qiao S. *Adv Mater*, 2020, 32: 2006784
59 Gowdru SM, Lin CH, Chang CC, Chen YC, Kuo YL, Chang CC, Patil SB, Pao CW, Chen JL, Lee CR, Chang CK, Chuang YC, Sheu HS, Yang CI, Wang DY. *ACS Sustain Chem Eng*, 2022, 10: 12297–12306
60 Zheng W, Liu M, Lee LYS. *ACS Catal*, 2020, 10: 81–92
61 Zhang K, Zhu Y, Yue K, Zhan K, Wang P, Kong Y, Yan Y, Wang X. *Nano Res*, 2022, :
62 Wang B, Shang J, Guo C, Zhang J, Zhu F, Han A, Liu J. *Small*, 2019, 15: 1804761
63 Wang B, Han X, Guo C, Jing J, Yang C, Li Y, Han A, Wang D, Liu J. *Appl Catal B-Environ*, 2021, 298: 120580
64 Wang Y, Yan L, Dastafkan K, Zhao C, Zhao X, Xue Y, Huo J, Li S,

Zhai Q. *Adv Mater*, 2021, 33: 2006351
65 Huo J, Wang Y, Yan L, Xue Y, Li S, Hu M, Jiang Y, Zhai QG. *Nanoscale*, 2020, 12: 14514–14523
66 Senthil Raja D, Chuah XF, Lu SY. *Adv Energy Mater*, 2018, 8: 1801065
67 Huang H, Zhao Y, Bai Y, Li F, Zhang Y, Chen Y. *Adv Sci*, 2020, 7: 2000012
68 Chen Y, Wang J, Yu Z, Hou Y, Jiang R, Wang M, Huang J, Chen J, Zhang Y, Zhu H. *Appl Catal B-Environ*, 2022, 307: 121151
69 Stock N, Biswas S. *Chem Rev*, 2012, 112: 933–969
70 Feng L, Wang KY, Powell J, Zhou HC. *Matter*, 2019, 1: 801–824
71 Cai X, Xie Z, Li D, Kassymova M, Zang SQ, Jiang HL. *Coord Chem Rev*, 2020, 417: 213366
72 Chen X, Shao B, Tang MJ, He XL, Yang FJ, Guo ZP, Zhang Z, He CT, Huang FP, Huang J. *J Mater Chem A*, 2021, 9: 14682–14690
73 Liu YL, Liu XY, Feng L, Shao LX, Li SJ, Tang J, Cheng H, Chen Z, Huang R, Xu HC, Zhuang JL. *ChemSusChem*, 2022, 15: e202102603
74 Cai M, Liu Q, Xue Z, Li Y, Fan Y, Huang A, Li MR, Croft M, Tyson TA, Ke Z, Li G. *J Mater Chem A*, 2020, 8: 190–195
75 Li FL, Wang P, Huang X, Young DJ, Wang HF, Braunstein P, Lang JP. *Angew Chem Int Ed*, 2019, 58: 7051–7056
76 Senthil Raja D, Lin HW, Lu SY. *Nano Energy*, 2019, 57: 1–13
77 Li XF, Lu MY, Yu HY, Zhang TH, Liu J, Tian JH, Yang R. *ChemElectroChem*, 2019, 6: 4507–4510
78 Wang L, Wu Y, Cao R, Ren L, Chen M, Feng X, Zhou J, Wang B. *ACS Appl Mater Interfaces*, 2016, 8: 16736–16743
79 Liang J, Gao X, Guo B, Ding Y, Yan J, Guo Z, Tse ECM, Liu J. *Angew Chem Int Ed*, 2021, 60: 12770–12774
80 Liu S, Zhang C, Sun Y, Chen Q, He L, Zhang K, Zhang J, Liu B, Chen LF. *Coord Chem Rev*, 2020, 413: 213266
81 Wang S, Wang X. *Small*, 2015, 11: 3097–3112
82 Wu YP, Zhou W, Zhao J, Dong WW, Lan YQ, Li DS, Sun C, Bu X. *Angew Chem Int Ed*, 2017, 56: 13001–13005
83 Bucci A, Mondal SS, Martin-Diaconescu V, Shafir A, Lloret-Fillol J. *ACS Appl Energy Mater*, 2019, 2: 8930–8938
84 Liu M, Kong L, Wang X, He J, Bu XH. *Small*, 2019, 15: 1903410
85 Shahbazi Farahani F, Rahmanifar MS, Noori A, El-Kady MF, Hassani N, Neek-Amal M, Kaner RB, Mousavi MF. *J Am Chem Soc*, 2022, 144: 3411–3428
86 Cao C, Ma DD, Xu Q, Wu XT, Zhu QL. *Adv Funct Mater*, 2019, 29: 1807418
87 Rui K, Zhao G, Chen Y, Lin Y, Zhou Q, Chen J, Zhu J, Sun W, Huang W, Dou SX. *Adv Funct Mater*, 2018, 28: 1801554
88 Li S, Gao Y, Li N, Ge L, Bu X, Feng P. *Energy Environ Sci*, 2021, 14: 1897–1927
89 Luo X, Abazari R, Tahir M, Fan WK, Kumar A, Kalhorizadeh T, Kirillov AM, Amani-Ghadim AR, Chen J, Zhou Y. *Coord Chem Rev*, 2022, 461: 214505
90 Zhao X, Xue Z, Chen W, Bai X, Shi R, Mu T. *J Mater Chem A*, 2019, 7: 26238–26242
91 Xu S, Li M, Wang H, Sun Y, Liu W, Duan J, Chen S. *J Phys Chem C*, 2022, 126: 14094–14102
92 Zhao X, Pattengale B, Fan D, Zou Z, Zhao Y, Du J, Huang J, Xu C. *ACS Energy Lett*, 2018, 3: 2520–2526
93 Li Y, Ma W, Yang H, Tian Q, Xu Q, Han B. *Chem Commun*, 2022, 58: 6833–6836
94 Qiu Q, Wang T, Jing L, Huang K, Qin D. *Int J Hydrogen Energy*, 2020, 45: 11077–11088
95 Wang XL, Dong LZ, Qiao M, Tang YJ, Liu J, Li Y, Li SL, Su JX, Lan YQ. *Angew Chem Int Ed*, 2018, 57: 9660–9664
96 Xue Z, Li Y, Zhang Y, Geng W, Jia B, Tang J, Bao S, Wang HP, Fan Y, Wei Z, Zhang Z, Ke Z, Li G, Su CY. *Adv Energy Mater*, 2018, 8: 1801564
97 Huang L, Gao G, Zhang H, Chen J, Fang Y, Dong S. *Nano Energy*, 2020, 68: 104296
98 Fang M, Gao X, Liang J, Guo B, Zou L, Lu J, Gao Y, Tse ECM, Liu J. *J Mater Chem A*, 2022, 10: 7013–7019
99 Li S, Wang T, Tang D, Yang Y, Tian Y, Cui F, Sun J, Jing X, Sholl DS, Zhu G. *Adv Sci*, 2022, 9: 2203712
100 Li FL, Shao Q, Huang X, Lang JP. *Angew Chem Int Ed*, 2018, 57: 1888–1892
101 Li Z, Deng S, Yu H, Yin Z, Qi S, Yang L, Lv J, Sun Z, Zhang M. *J Mater Chem A*, 2022, 10: 4230–4241
102 Yue K, Liu J, Zhu Y, Xia C, Wang P, Zhang J, Kong Y, Wang X, Yan Y, Xia BY. *Energy Environ Sci*, 2021, 14: 6546–6553
103 Qian Q, Li Y, Liu Y, Yu L, Zhang G. *Adv Mater*, 2019, 31: 1901139
104 Han L, Xu J, Zhu X, Yang F, Jia X. *Mater Today Energy*, 2020, 16: 100419
105 Wang Y, Wang B, Liu X, Wang Y, Wang Y, Liu Z. *ACS Appl Energy Mater*, 2022, 5: 8686–8696
106 Li F, Jiang M, Lai C, Xu H, Zhang K, Jin Z. *Nano Lett*, 2022, 22: 7238–7245
107 Zhuang L, Ge L, Liu H, Jiang Z, Jia Y, Li Z, Yang D, Hocking RK, Li M, Zhang L, Wang X, Yao X, Zhu Z. *Angew Chem Int Ed*, 2019, 58: 13565–13572
108 Dhakshinamoorthy A, Asiri AM, Garcia H. *Adv Mater*, 2019, 31: 1900617
109 Zhao S, Wang Y, Dong J, He CT, Yin H, An P, Zhao K, Zhang X, Gao C, Zhang L, Lv J, Wang J, Zhang J, Khattak AM, Khan NA, Wei Z, Zhang J, Liu S, Zhao H, Tang Z. *Nat Energy*, 2016, 1: 16184
110 Huang J, Li Y, Huang RK, He CT, Gong L, Hu Q, Wang L, Xu YT, Tian XY, Liu SY, Ye ZM, Wang F, Zhou DD, Zhang WX, Zhang JP. *Angew Chem Int Ed*, 2018, 57: 4632–4636
111 Liu Y, Li X, Sun Q, Wang Z, Huang WH, Guo X, Fan Z, Ye R, Zhu Y, Chueh CC, Chen CL, Zhu Z. *Small*, 2022, 18: 2201076
112 Zhang W, Wang Y, Zheng H, Li R, Tang Y, Li B, Zhu C, You L, Gao MR, Liu Z, Yu SH, Zhou K. *ACS Nano*, 2020, 14: 1971–1981
113 Zhao ZY, Sun X, Gu H, Niu Z, Braunstein P, Lang JP. *ACS Appl Mater Interfaces*, 2022, 14: 15133–15140
114 Zhao L, Dong B, Li S, Zhou L, Lai L, Wang Z, Zhao S, Han M, Gao K, Lu M, Xie X, Chen B, Liu Z, Wang X, Zhang H, Li H, Liu J, Zhang H, Huang X, Huang W. *ACS Nano*, 2017, 11: 5800–5807
115 Zhu B, Wen D, Liang Z, Zou R. *Coord Chem Rev*, 2021, 446: 214119
116 Zhang M, Zheng BH, Xu J, Pan N, Yu J, Chen M, Cao H. *Chem Commun*, 2018, 54: 13579–13582
117 Sun Y, Ding S, Xu S, Duan J, Chen S. *J Power Sources*, 2021, 494: 229733
118 Lin L, Zhang Q, Ni Y, Shang L, Zhang X, Yan Z, Zhao Q, Chen J. *Chem*, 2022, 8: 1822–1854
119 Zhong H, Wang M, Chen G, Dong R, Feng X. *ACS Nano*, 2022, 16: 1759–1780
120 Li C, Zhang L, Chen J, Li X, Sun J, Zhu J, Wang X, Fu Y. *Nanoscale*, 2021, 13: 485–509
121 Miner EM, Gul S, Ricke ND, Pastor E, Yano J, Yachandra VK, Van Voorhis T, Dincă M. *ACS Catal*, 2017, 7: 7726–7731
122 Takaishi S, Hosoda M, Kajiwara T, Miyasaka H, Yamashita M, Nakanishi Y, Kitagawa Y, Yamaguchi K, Kobayashi A, Kitagawa H. *Inorg Chem*, 2009, 48: 9048–9050
123 Huang X, Yao H, Cui Y, Hao W, Zhu J, Xu W, Zhu D. *ACS Appl Mater Interfaces*, 2017, 9: 40752–40759
124 Jia H, Yao Y, Zhao J, Gao Y, Luo Z, Du P. *J Mater Chem A*, 2018, 6: 1188–1195
125 Li J, Liu P, Mao J, Yan J, Song W. *J Mater Chem A*, 2021, 9: 1623–1629
126 Li C, Shi L, Zhang L, Chen P, Zhu J, Wang X, Fu Y. *J Mater Chem A*, 2020, 8: 369–379
127 Shi X, Hua R, Xu Y, Liu T, Lu G. *Sustain Energy Fuels*, 2020, 4: 4589–4597
128 Yu S, Wu Y, Xue Q, Zhu JJ, Zhou Y. *J Mater Chem A*, 2022, 10: 4936–4943
129 Tang YJ, Chen Y, Zhu HJ, Zhang AM, Wang XL, Dong LZ, Li SL, Xu Q, Lan YQ. *J Mater Chem A*, 2018, 6: 21969–21977
130 Cai G, Zhang W, Jiao L, Yu SH, Jiang HL. *Chem*, 2017, 2: 791–802
131 Tang YJ, Zheng H, Wang Y, Zhang W, Zhou K. *Adv Funct Mater*,

2021, 31: 2102648
132 Luo P, Li S, Zhao Y, Ye G, Wei C, Hu Y, Wei C. *ChemCatChem*, 2019, 11: 6061–6069
133 Sun F, Wang G, Ding Y, Wang C, Yuan B, Lin Y. *Adv Energy Mater*, 2018, 8: 1800584
134 Meng C, Cao Y, Luo Y, Zhang F, Kong Q, Alshehri AA, Alzahrani KA, Li T, Liu Q, Sun X. *Inorg Chem Front*, 2021, 8: 3007–3011
135 Cheng W, Zhao X, Su H, Tang F, Che W, Zhang H, Liu Q. *Nat Energy*, 2019, 4: 115–122
136 Wang CP, Feng Y, Sun H, Wang Y, Yin J, Yao Z, Bu XH, Zhu J. *ACS Catal*, 2021, 11: 7132–7143
137 Li DJ, Li QH, Gu ZG, Zhang J. *J Mater Chem A*, 2019, 7: 18519–18528
138 Song J, Zhao S, Liu D, Xiong Y, Hu F, Li L, Li L, Pan H, Peng S. *Chem Commun*, 2022, 58: 9662–9665
139 Wang ZH, Wang XF, Tan Z, Song XZ. *Mater Today Energy*, 2021, 19: 100618
140 Li N, Liu J, Dong BX, Lan YQ. *Angew Chem Int Ed*, 2020, 59: 20779–20793
141 Du DY, Qin JS, Li SL, Su ZM, Lan YQ. *Chem Soc Rev*, 2014, 43: 4615–4632
142 Mukhopadhyay S, Debgupta J, Singh C, Kar A, Das SK. *Angew Chem Int Ed*, 2018, 57: 1918–1923
143 Samaniyan M, Mirzaei M, Khajavian R, Eshtiagh-Hosseini H, Streb C. *ACS Catal*, 2019, 9: 10174–10191
144 Zhang S, Ou F, Ning S, Cheng P. *Inorg Chem Front*, 2021, 8: 1865–1899
145 Nohra B, El Moll H, Rodriguez Albelo LM, Mialane P, Marrot J, Mellot-Draznieks C, O'Keeffe M, Ngo Biboum R, Lemaire J, Keita B, Nadjo L, Dolbecq A. *J Am Chem Soc*, 2011, 133: 13363–13374
146 Qin JS, Du DY, Guan W, Bo XJ, Li YF, Guo LP, Su ZM, Wang YY, Lan YQ, Zhou HC. *J Am Chem Soc*, 2015, 137: 7169–7177
147 Wang L, Wang AN, Xue ZZ, Wang YR, Han SD, Wang GM. *Chin Chem Lett*, 2022, :
148 Zhang L, Li S, Gómez-García CJ, Ma H, Zhang C, Pang H, Li B. *ACS Appl Mater Interfaces*, 2018, 10: 31498–31504
149 Abdelkader-Fernández VK, Fernandes DM, Balula SS, Cunha-Silva L, Freire C. *J Mater Chem A*, 2020, 8: 13509–13521
150 Wang X, Luo JY, Tian JW, Huang DD, Wu YP, Li S, Li DS. *Inorg Chem Commun*, 2018, 98: 141–144
151 Chen K, Ray D, Ziebel ME, Gaggioli CA, Gagliardi L, Marinescu SC. *ACS Appl Mater Interfaces*, 2021, 13: 34419–34427
152 Ding YX, Zheng QH, Peng MT, Chen C, Zou KF, Dong BX, Liu WL, Teng YL. *Catal Commun*, 2021, 161: 106367
153 Chen C, Suo N, Han X, He X, Dou Z, Lin Z, Cui L. *J Alloys Compd*, 2021, 865: 158795
154 Kong Y, Xiong D, Lu C, Wang J, Liu T, Ying S, Ma X, Yi FY. *ACS Appl Mater Interfaces*, 2022, 14: 37804–37813